Dilepton Radiation at the CERN Super Proton Synchrotron

Hendrik van Hees and Ralf Rapp

Cyclotron Institute and Physics Department, Texas A&M University, College Station, Texas 77843-3366, USA
(Dated: August 24, 2011)

A quantitative evaluation of dilepton sources in heavy-ion reactions is performed taking into account both thermal and non-thermal production mechanisms. The hadronic thermal emission rate is based on an electromagnetic current-correlation function with a low-mass region (LMR, $M \lesssim 1$ GeV) dominated by vector mesons (ρ, ω, ϕ) and an intermediate-mass region (IMR, 1 GeV $\leq M \leq 3$ GeV) characterized by (the onset of) a multi-meson continuum. A convolution of the emission rates over a thermal fireball expansion results in good agreement with experiment in the low-mass spectra, confirming the predicted broadening of the ρ meson in hadronic matter in connection with the prevalence of baryon-induced medium effects. The absolute magnitude of the LMR excess is mostly controlled by the fireball lifetime, which in turn leads to a consistent explanation of the dilepton excess in the IMR in terms of thermal radiation. The analysis of experimental transverse-momentum (q_T) spectra reveals discrepancies with thermal emission for $q_T \gtrsim 1$ GeV in noncentral In-In collisions, which we address by extending our calculations by: (i) a refined treatment of ρ decays at thermal freezeout, (ii) primordially produced ρ's subject to energy-loss, (iii) Drell-Yan annihilation, and (iv) thermal radiation from t-channel meson exchange processes. We investigate the sensitivity of dilepton spectra to the critical temperature and hadro-chemical freezeout of the fireball. The ρ broadening in the LMR turns out to be robust, while in the IMR Quark-Gluon Plasma radiation is moderate unless the critical temperature is rather low.

PACS numbers:

I. INTRODUCTION

Dilepton invariant-mass spectra provide the unique opportunity to directly probe the electromagnetic (e.m.) spectral function of the hot and dense medium created in energetic collisions of heavy nuclei [1–3]. In the low-mass region (LMR, $M \leq 1$ GeV), this enables the study of modifications of the light vector mesons (V=ρ, ω, ϕ) caused by their interactions with the surrounding matter particles and/or changes in the underlying condensate structure. In the intermediate-mass region (IMR, 1 GeV $\leq M \leq 3$ GeV), electromagnetic emission is expected to become continuum-like with rather well-defined strength rendering it a suitable tool to infer temperatures of the excited system (well) before interactions cease ("thermal freezeout").

Dilepton measurements in heavy-ion collisions at the CERN-SPS (at center-of-mass energies of $\sqrt{s}$=17.3 and 8.8 AGeV) have proven the presence of substantial excess radiation beyond e.m. final-state decays of produced hadrons in both the LMR [4, 5] and IMR [6–8]. This, in particular, corroborated the presence of interacting *matter* over a duration of ∼10-15 fm/c in central Pb-Au collisions. Moreover, the spectral shape of the excess in the LMR could only be accounted for if major medium modifications of the vacuum ρ-meson line shape were incorporated [1–3]. Both the implementation of a dropping mass or a strong broadening of its width as following from hadronic many-body approaches, were compatible with the large enhancement observed at masses below the free ρ mass. In addition, with the same underlying fireball model (lifetime and temperature evolution), reasonable agreement with the enhancement measured in the IMR [7, 8] has been established [9] (as well as with direct photon spectra [10, 11]). The excess for $M \geq 1.5$ GeV was largely attributed to four-pion type annihilations in the hadronic phase, with a strength determined by the vacuum e.m. spectral function, while the calculated Quark-Gluon Plasma (QGP) contribution to the thermal yield amounted to ∼30% (∼10-20% in the LMR [12]).

A recent, substantial, improvement in statistics and mass resolution in low-mass dimuon spectra in In-In collisions [13] shows good agreement with predictions for thermal radiation with in-medium ρ-meson broadening as following from hadronic many-body calculations [12, 14]. The shape of the excess radiation is well described from threshold ($M = 2m_\mu$) to $M \simeq 0.9$ GeV, while the absolute yield is overpredicted by about 30%. The latter can be accommodated by a minor adjustment in the thermal fireball evolution (amounting to a 30% lower fireball lifetime), and after inclusion of in-medium ω and ϕ decays (whose contribution is mostly localized around their free mass), as well as four-pion type annihilation (which sets in at masses $M \gtrsim 0.9$ GeV), a quantitative description of the NA60 invariant-mass spectra from threshold to ∼1.4 GeV in central In-In collisions emerges [15] (see also Refs. [16, 17]). While the inclusive mass spectra are well described, the comparison of the calculations with newly released transverse pair-momentum (q_T) spectra [18] reveals some discrepancies at $q_T > 1$ GeV in semicentral In-In.

In the present article we reiterate the main points of our previous study of dilepton invariant-mass spectra at the SPS, and extend the analysis to q_T spectra. In particular, we conduct a detailed analysis of sources at high

q_T, in terms of (i) an improved treatment of ρ decays at thermal freezeout (which are subject to maximal blue shift due to transverse flow), (ii) a component of primordial (hard-produced) ρ mesons subject to energy loss when traversing the medium (using high-p_T pion spectra as a guideline), (iii) Drell-Yan (DY) annihilation in primordial N-N collisions which we extrapolate to small mass by imposing constraints from real photon production, and (iv) meson t-channel exchange contributions to the thermal production rate which are not included in the many-body vector-meson spectral functions (but which have been found to be a significant source at high q_T in real photon production [11])[1]. Another interesting issue which has received little attention thus far is how uncertainties in the critical temperature and hadrochemical evolution of the fireball affect dilepton spectra. For hadro-chemical freezeout we investigate the sensitivity to temperatures in the range $T_{\rm ch} \simeq$ 160-175 MeV, representative for top SPS energy according to recent thermal model analyses [21, 22]. In connection with updates of lattice-QCD results indicating a critical temperature up to $T_c \simeq$ 190-200 MeV [23], this, in particular, opens the possibility of a chemically equilibrated hot and dense hadronic phase for, say, T = 160-190 MeV, which we also consider. We furthermore conduct a quantitative study of effective slope parameters of the NA60 q_T spectra, where the investigations of the fireball chemistry are supplemented with variations of the transverse flow velocity. Finally, we revisit the consequences of our fireball refinements on our previous evaluations [24] of dielectron spectra as measured by CERES/NA45 in semicentral Pb-Au collisions [4], as well as recent data in central Pb-Au [25].

Our article is organized as follows: in Sec. II we recall the main ingredients of our approach to calculate thermal emission rates, based on the e.m. spectral function in the vacuum (Sec. II A), followed by discussing medium effects on hadronic emission at low mass (due to in-medium ρ, ω and ϕ spectral functions; Sec. II B) and at intermediate mass (due to finite-T chiral mixing; Sec. II C); a new element not included in previous spectral-function calculations are t-channel meson-exchange reactions which therefore are elaborated in more detail in Sec. II D, while we will be brief on partonic emission from a Quark-Gluon Plasma (Sec. II E). In Sec. III we evaluate nonthermal dilepton sources: ρ-meson decays at thermal freezeout (whose decay kinematics differ from thermal radiation; Sec. III A), an estimate of primordial ρ's at large q_T (which do not thermalize; Sec. III B), and Drell-Yan annihilation (with an extrapolation to low mass; Sec. III C). In Sec. IV we recollect the ingredients to our thermal fireball model for the space-time evolution of the medium in heavy-ion collisions, including variations in hadrochemical freezeout and critical temperature. In Sec. V we implement all dilepton sources into the fireball to compute dimuon invariant-mass (Sec. V A) and transverse-momentum spectra (Sec. V B) in comparison to NA60 data; the effect of hadrochemistry and T_c on NA60 spectra is worked out in Sec. V C, followed by a slope analysis of q_T spectra (Sec. V D) in the context of which we also investigate different radial flow scenarios; the improvements in the fireball and dilepton source description as deduced from the NA60 data are confronted with previous and new CERES/NA45 data in Sec. V E. Sec. VI contains a summary and conclusions.

[1] Note that contributions (ii)-(iv) have little bearing on the inclusive invariant-mass spectra which are predominantly populated by low-momentum sources with $q_T \lesssim 1$ GeV. Therefore, the inclusion of these contributions does not upset our earlier description of inclusive M spectra in terms of thermal radiation and freezeout ρ's. Initial results of these studies have been reported in Refs. [19, 20].

II. THERMAL DILEPTON RADIATION

A. Emission Rate and Electromagnetic Spectral Function

In thermal equilibrium the rate of dilepton emission per four-volume and four-momentum can be related to the hadronic e.m. spectral function as [26]

$$\frac{{\rm d}N_{ll}}{{\rm d}^4x{\rm d}^4q} = -\frac{\alpha^2}{3\pi^3}\frac{L(M^2)}{M^2}\,{\rm Im}\,\Pi^{\mu}_{{\rm em},\mu}(M,q;\mu_B,T) \times f^B(q_0;T)\ , \tag{1}$$

which in this article we will refer to as thermal dileptons (or thermal radiation). The retarded e.m. current-current correlator is given by

$$\Pi^{\mu\nu}_{\rm em}(q) = {\rm i}\int {\rm d}^4x {\rm e}^{{\rm i}q_\sigma x^\sigma}\Theta(x^0)\,\langle[\mathbf{J}^\mu_{\rm em}(x),\mathbf{J}^\nu_{\rm em}(0)]\rangle\ , \tag{2}$$

where α=$e^2/(4\pi)$=1/137 denotes the fine structure constant, $M^2 = q_0^2 - q^2$ the dilepton invariant mass squared with energy q_0 and three-momentum q, and $f^B(q_0;T)$ the thermal Bose distribution function (T: temperature, μ_B: baryon chemical potential). The final-state lepton phase space factor,

$$L(M) = \left(1+\frac{2m_l^2}{M^2}\right)\sqrt{1-\frac{4m_l^2}{M^2}}\ , \tag{3}$$

depends on the lepton mass, m_l=0.511(105.6) MeV for electrons (muons; $l = e,\mu$), but quickly approaches one above threshold, $M = 2m_l$ (*e.g.*, $L(M = 0.3\,{\rm GeV}) = 0.89$ for dimuons).

In the vacuum, the e.m. spectral function, ${\rm Im}\,\Pi_{\rm em}(M)$, is well known from e^+e^- annihilation into hadrons. It is characterized by the light vector resonances $\rho(770)$, $\omega(782)$ and $\phi(1020)$ at low mass (vector dominance model (VDM)) and a perturbative quark-antiquark continuum

at higher mass,

$$\mathrm{Im}\,\Pi_{\rm em} = \begin{cases} \sum\limits_{V=\rho,\omega,\phi} \left(\frac{m_V^2}{g_V}\right)^2 \mathrm{Im}\,D_V\,, & M \lesssim M_{\rm dual} \\ -\frac{N_c M^2}{12\pi}\,(1+\frac{\alpha_s}{\pi}+\dots)\sum\limits_i (e_i)^2\,, & M \gtrsim M_{\rm dual} \end{cases} \tag{4}$$

($N_c = 3$: number of colors, α_s: strong coupling constant, e_i: the electric quark charge in units of the electron charge, and i is running over up, down and strange quark flavors for $M < 3$ GeV). $M_{\rm dual} \simeq 1.5$ GeV signifies a "duality" scale above which the total cross section for $e^+e^- \to$ hadrons (and thus the strength of $\mathrm{Im}\,\Pi_{\rm em}$) essentially behaves perturbatively with little impact from subsequent hadronization. Since the hadronic final state in e^+e^- annihilation approximately resembles a thermal medium (except for strangeness), time-reversal invariance of strong and electromagnetic interactions implies that, to leading order in temperature, the equilibrium dilepton emission rate of hadronic matter is determined by the free e.m. correlator, $\Pi_{\rm em}^{\rm vac}$, cf. also Refs. [9, 27].

In the hadronic basis, the e.m. spectral function is dominated by the isovector (ρ) channel while the isoscalar channels are suppressed. The SU(3)-flavor quark model, *e.g.*, predicts a weighting of 9:1:2 for the e.m. couplings of ρ, ω and ϕ, respectively. These values are roughly in line with the electromagnetic decay widths $\Gamma_{V\to ee} = \frac{4\pi\alpha^2}{3} m_V/g_V^2 = 7.0$, 0.60 and 1.27 keV for ρ, ω and ϕ, respectively (the empirical values of the ϕ width should be corrected for phase space by the ratio m_ω/m_ϕ=0.77).

The vector-isovector channel furthermore provides the most direct link to chiral symmetry: under chiral rotations, the ρ channel transforms into the axialvector-isovector (a_1) one. Thus, the a_1 is commonly identified as the chiral partner of the ρ.[2] The pertinent spectral functions in free space have been accurately measured in hadronic τ decays [29, 30], cf. Fig. 1, and evaluated in terms of chiral order parameters (f_π, four-quark condensates) using Weinberg sum rules [31, 32]. To leading order in temperature (*i.e.*, for a hot pion gas), the mutual in-medium modifications of vector and axialvector channels can be inferred from chiral symmetry alone, as will be discussed in Sec. II C below.

The main objective for the remainder of this Section is a realistic evaluation of the in-medium e.m. spectral function. In the LMR, we assume that vector dominance remains valid in the medium. Our calculations of the V-meson spectral functions, $A_V = -2\,\mathrm{Im}\,D_V$, utilize effective hadronic Lagrangians, where the interaction vertices and coupling constants are constrained by gauge and chiral symmetry, as well as empirical decay and scattering data. Medium effects are calculated within hadronic many-body theory *without* introducing explicit medium dependencies of the bare parameters in the Lagrangian (which require information beyond the effective hadronic theory). A careful comparison of our predictions for dilepton spectra in heavy-ion collisions with experiment can then serve as a basis for identifying medium effects that go beyond the hadronic many-body framework.

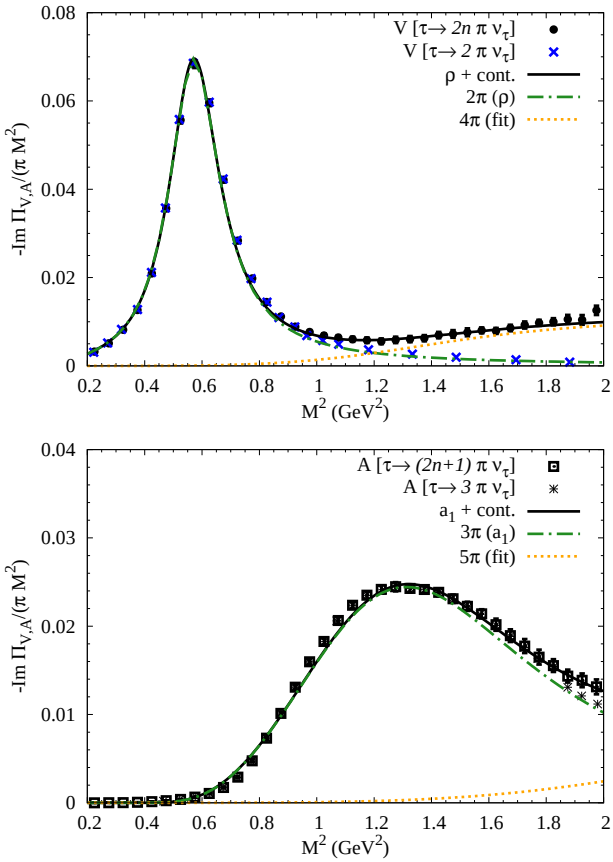

FIG. 1: (Color online) Free isovector-vector (upper panel) and -axialvector (lower panel) spectral functions as measured in hadronic τ-decays [29], compared to fits with three- and four-pion contributions (the two-pion piece follows from the previously calculated ρ propagator [33]).

B. Hadronic Emission at Low Mass: In-Medium Vector Mesons

Since the prevalent role in the LMR of the e.m. correlator is played by the ρ meson, the latter has been the main focus for studying in-medium effects in thermal dilepton production. However, with the current precision of the NA60 dilepton data on the 10-20% level, thermal emission from ω and ϕ decays becomes relevant. Their contributions are an inevitable consequence of the formation of a thermal medium, and we therefore incorporate

[2] An alternative has recently been suggested in Ref. [28] in terms of the "Vector Manifestation" (VM) of chiral symmetry, where the chiral partner of the (longitudinal) ρ is identified with the pion.

them along with pertinent medium modifications.

Within the VDM the in-medium e.m. correlator in the LMR remains directly proportional to the vector-meson spectral functions as in Eq. (4). The key objective is then to calculate the vector-meson selfenergies at finite temperature and baryon density (ϱ_B), Σ_V, figuring into the propagator as

$$D_V = \frac{1}{M^2 - (m_V^{(0)})^2 - \Sigma_{VP} - \Sigma_{VM} - \Sigma_{VB}} \,. \qquad (5)$$

Here, $m_V^{(0)}$ denotes the bare mass, and the selfenergy contributions are classified into three types: (i) medium modifications of the pseudoscalar meson cloud, Σ_{VP} ($P = \pi\pi$, 3π or $K\bar{K}$ for $V = \rho$, ω or ϕ, respectively), and direct interactions of V with (ii) mesons and (iii) baryons from the surrounding heat bath, Σ_{VM} and Σ_{VB}. One should also note that without the implementation of a phase transition into a realistic hadronic model (which has not been achieved thus far), many-body calculations are to be considered as an extrapolation beyond a certain temperature and/or density. We estimate that, under SPS conditions, our approach should be reliable up to temperatures of about $T \simeq 150$ MeV, where the total hadron density amounts to about $\varrho_h \simeq 2\varrho_0$ (with a net-baryon density of about $0.7\varrho_0$), while it has increased to about $5\varrho_0$ at the expected phase boundary at $T_c \simeq 175$ MeV. In the following we briefly recall the construction of, and constraints on, the underlying effective Lagrangians.

1. ρ Meson

The first step in the calculation of a realistic ρ propagator is a proper description of its coupling to the pion cloud in vacuum (giving rise to its two-pion decay width, $\Gamma_{\rho\pi\pi}(m_\rho) \simeq 150$ MeV). A suitable chiral effective Lagrangian can be obtained by, *e.g.*, introducing the vector fields as local gauge fields into the chiral pion Lagrangians and implementing the photon field via vector dominance [34, 35],

$$\begin{aligned}\mathcal{L}_{\pi\rho\gamma} =& g_\rho \vec{\rho}_\mu \cdot (\vec{\pi} \times \partial^\mu \vec{\pi}) \\ & - \frac{1}{2} g_\rho^2 \left[\vec{\rho}_\mu \cdot \vec{\rho}^\mu \vec{\pi}^2 - \vec{\rho}^\mu \cdot \vec{\pi} \vec{\rho}_\mu \cdot \vec{\pi}\right] \\ & + \frac{e m_\rho^2}{g_\rho} A_\mu \rho_3^\mu \,. \end{aligned} \qquad (6)$$

The pertinent two-pion and one-pion-tadpole diagrams specify the ρ's pion cloud in the vacuum with a transverse selfenergy (using a proper regularization procedure). The coupling constant, g_ρ, a cutoff parameter, Λ_ρ (to render the pion loops finite), and the bare ρ-mass, $m_\rho^{(0)}$, can be readily adjusted to reproduce P-wave π-π scattering phase shifts and the pion e.m. formfactor in free space [33]. This model also predicts the two-pion part of the τ-decay data well, cf. Fig. 1.

Based on the above model in the vacuum, we adopt the in-medium ρ propagator from the hadronic many-body approach developed in Refs. [24, 33, 36], to which we refer the reader for more details. Modifications of the pion cloud are induced by an in-medium π propagator which is dressed with standard NN^{-1} and ΔN^{-1} excitations in nuclear matter, supplemented with appropriate vertex corrections to maintain a conserved vector current. While the calculations of nuclear pion-cloud modifications are often restricted to the case of vanishing ρ three-momentum ("back-to-back" kinematics), we here employ the extension to finite three-momentum worked out in Ref. [33]. This is particularly important in that it enables (i) to constrain the corresponding medium effects by nuclear photo-absorption data [37] and $\pi N \to \rho N$ scattering, and (ii) a meaningful application to dilepton transverse momentum spectra. At finite temperature, where a (large) fraction of nucleons is thermally excited into baryons, only the nucleon density should be employed. To account for (i) $\pi B N^{-1}$ excitations into higher resonances and (ii) $\pi B_2 B_1^{-1}$ excitations ($B_1 \neq N$), an "effective" nucleon density $\varrho_N^{\rm eff} \equiv \varrho_N + 0.5\varrho_B$ ($B \neq N$) has been used in the pion propagators [24] (we estimate the uncertainty implied by this prescription to be about $\pm 10\%$). In addition, effects of antibaryons are added by multiplying $\varrho_N^{\rm eff}$ with a factor $(1 + \bar{p}/p)$ where $\bar{p}/p$ denotes the measured antiproton-to-proton ratio (this is a small correction at SPS energies but becomes essential at RHIC [38]). The modifications of the pion cloud induced by a pion gas have been found to be rather small in various analyses [39–43]. A large part of the pion-gas effect is already provided by the Bose enhancement factor, $[1 + f^\pi(\omega_1) + f^\pi(\omega_2)]$ [41], while low-energy π-π interactions are suppressed by chiral symmetry. The former is included in the present calculations, but the latter are neglected (being much weaker than baryon-induced effects).

Direct interactions of the (bare) ρ with baryons and mesons have been approximated by resonance interactions (pion-exchange interactions, including spacelike pions, are implicit in the nuclear modifications of the pion-cloud part). For $\rho + N \to B$ (*i.e.*, $\rho B N^{-1}$ excitations), this includes both S-wave scattering into negative-parity baryons and P-wave scattering into positive-parity baryons, with $B = N(1520)$, $\Delta(1620)$, $\Delta(1700)$ and N, $\Delta(1232)$, $N(1440)$, $N(1720)$, $\Delta(1905)$, $N(2000)$, respectively. An estimate of the involved couplings and cutoff parameters can be obtained by reproducing the empirical $B \to \rho N, \gamma N$ decay widths, but more reliable constraints follow from comprehensive scattering data. For the present model, in addition to hadronic decay branchings, cold nuclear matter effects induced in both the pion cloud and via resonant ρ-N interactions have been checked against total photoabsorption cross sections on the nucleon and nuclei [37], as well as $\pi N \to \rho N$ scattering data [1, 44]. Whereas γN and ρN scattering

relates to the low-density limit of the ρ-spectral function, γA data constrain $\mathrm{Im}\, D_\rho(M \to 0, q)$ close to nuclear saturation density, $\varrho_0 = 0.16$ fm^{-3}. For the finite-temperature case, excitations on hyperons of the type $\rho Y_2 Y_1^{-1}$ are incorporated for $Y_1 = \Lambda(1115)$, $\Sigma(1192)$ and Y_2 resonances with quantum numbers equivalent to the nonstrange sector and appreciable empirical decay widths into ρ's and/or photons. $\rho B_2 B_1^{-1}$ excitations on thermally excited nonstrange baryons (*e.g.*, $\Delta(1930)\Delta^{-1}$) are included but turned out to be small.

In the meson gas, direct ρ-M interactions on thermal mesons ($M = \pi$, K, ρ) have been scrutinized in Ref. [45], again based on s-channel resonance dominance, $\rho M \to R$, and with pertinent Lagrangians satisfying basic requirements of vector-current conservation and chiral symmetry. As in the case of excited baryons, the couplings and cutoffs have been estimated from combined hadronic and radiative decay widths. The most important contributions to the ρ propagator arise from axialvector mesons, $R = a_1(1260)$ (chiral partner of the ρ), $h_1(1170)$ and $K_1(1270)$, as well as the $\omega(782)$.

Another valuable consistency check for the in-medium properties of hadrons are QCD sum rules. The latter relate a dispersion integral over a spectral function to an operator product expansion (OPE) for the correlation function at spacelike four-momenta, $q_\mu q^\mu < 0$. The nonperturbative coefficients of the OPE involve quark and gluon condensates whose in-medium modifications reflect upon (an energy integral over) the spectral function. Generically, a reduction of the condensates leads to a softening of the spectral function, *i.e.*, a shift of strength to lower mass. However, as has been elaborated in Ref. [46] for the case of cold nuclear matter, the additional low-mass strength in the in-medium ρ spectral function can be due to both a reduced mass or a broadening of the width, or a combination thereof. The pertinent "allowed band" for width and mass values at normal nuclear matter density has been quantified in Ref. [46]. For the ρ spectral function employed here [24], one finds a mass and width of $(m_\rho, \Gamma_\rho)|_{\varrho_0} \simeq (820, 450)$ MeV at nuclear saturation density and vanishing three-momentum. These values turn out to be consistent with the band derived in Ref. [46] (cf. middle panel of Fig. 2 in there), but more extensive (*i.e.*, different densities and temperatures) and quantitative comparisons are certainly desirable (*e.g.*, the low-mass strength (shoulder) in the ρ spectral function which is induced by "Pisobar" ($\pi\Delta N^{-1}$) and "Rhosobar" ($\rho B N^{-1}$) excitations, cannot be represented in Breit-Wigner form as underlying Ref. [46]). However, at this point, there is no indication for changes in the bare parameters in the Lagrangian, *i.e.*, at nuclear saturation density hadronic many-body effects saturate the reduction of quark and gluon condensates as required by QCD sum rules.

The ρ-spectral functions under fireball conditions representing the evolution of the hadronic phase at full SPS energy ($\sqrt{s} = 17.3$ AGeV) are displayed in the upper panel of Fig. 2. The resonance strongly broadens with little, if any, mass shift, essentially leading to its "melting" close to the expected phase boundary. These features are a rather generic consequence of a multilevel excitation spectrum in which real parts occur with altering signs while imaginary parts are negative definite and strictly

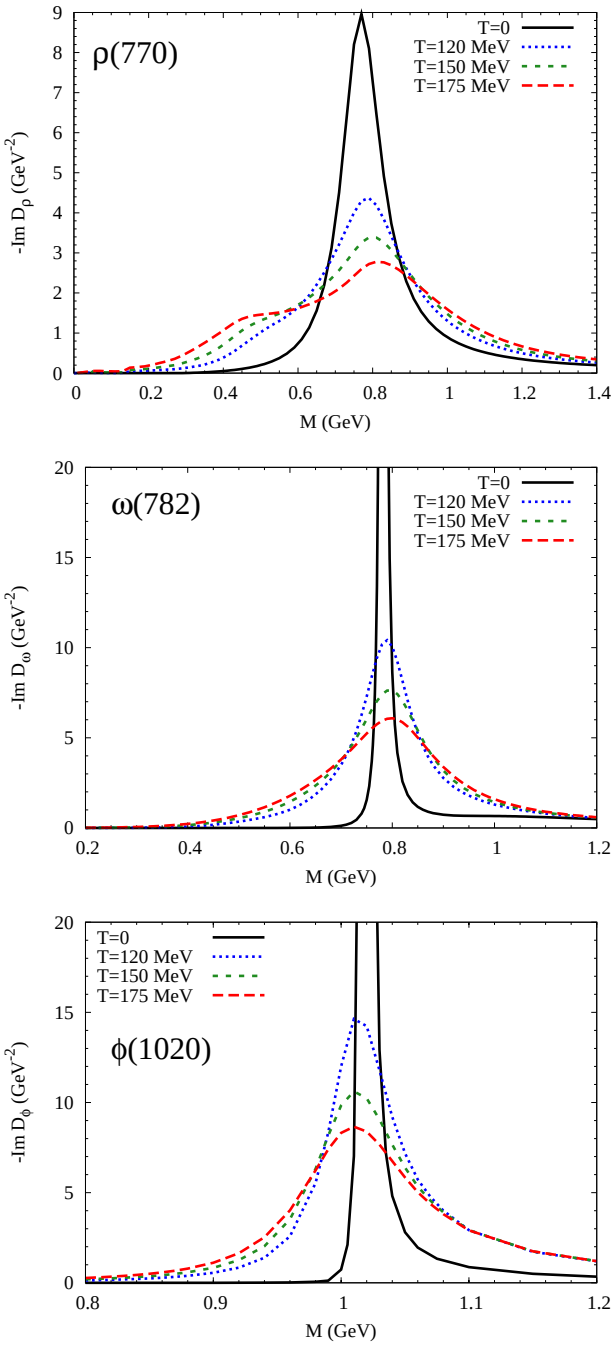

FIG. 2: (Color online) In-medium spectral functions of ρ (upper panel), ω (middle panel) and ϕ (lower panel) under conditions representative for the time evolution of heavy-ion collisions at full SPS energy: $(\mu_N, \mu_\pi, \mu_K, T)$ [MeV] $= (232, 0, 0, 175)$, $(331, 39, 62, 150)$, $(449, 79, 136, 120)$ and vacuum for the dotted, short-dashed, long-dashed and solid lines, respectively.

add up. Also note the development of a pronounced low-energy strength around $M = 0.4$ GeV which leads to a very large enhancement over the vacuum spectral function (and will be augmented by thermal Bose factors in the dilepton rate). At lower temperatures, the presence of meson-chemical potentials (for π, K, η) implies higher meson and baryon densities than in chemical equilibrium at a given temperature, entailing stronger medium effects. The build-up of the chemical potentials (necessary to preserve the experimentally observed hadron ratios throughout the hadronic cooling) therefore facilitates the observation of in-medium effects in the dilepton spectra. A strong broadening of the ρ in hot and dense matter has also been reported in other calculations at finite T and ϱ_B [47, 48].

The in-medium ρ-spectral function has been rather extensively employed to calculate dilepton spectra in heavy-ion collisions. At full SPS energy it has been implemented into fireball models [24, 36], transport simulations [49] and hydrodynamic evolutions [50], with fair success (and consistency) in describing CERES/NA45 data in central and semicentral Pb-Au collisions [4]. When averaged over a typical space-time evolution, the in-medium ρ width at SPS amounts to $\Gamma_\rho^{\rm med} \simeq 350$-400 MeV, almost three times its vacuum value, implying $\Gamma_\rho(T_c) \simeq m_\rho$ when extrapolated to the expected QCD-phase boundary. Despite an experimental pion-to-baryon ratio of $\sim 5:1$, medium effects induced by baryons have been identified as essential at SPS energies early on [36]. This has led to the prediction of an even larger excess at lower beam energies, which was tentatively confirmed in a 40 AGeV Pb+Au run of CERES/NA45 [5] (albeit with rather large errors). The lightlike limit of the ρ-spectral function has been applied to calculate thermal photon spectra [11], supplemented with meson-exchange reactions which are not included in Im D_ρ (these become significant at momenta above 1 GeV and will be discussed in Sec. II D below). After convolution over the same fireball model as used for dileptons, the direct-photon excess observed by WA98 in central Pb-Pb reactions at SPS [10], as well as by PHENIX in central Au-Au collisions at RHIC [51], can be reasonably well accounted for (with additional primordial and QGP photon sources, the latter being subdominant at SPS). The in-medium ρ-spectral function following from hadronic many-body theory [24] has thus passed a rather wide range of both theoretical and phenomenological tests, in both cold nuclear as well as hot hadronic matter.

2. ω Meson

Medium effects on the ω have received less attention so far, especially in the context of ultrarelativistic heavy-ion collisions (URHICs) where its dilepton decays are dominated by free decays after thermal freezeout (commonly referred to as a "cocktail" contribution). We here adopt the same approach as for the ρ, following Ref. [38]. In the vacuum, the hadronic ω width, $\Gamma_{\omega\to 3\pi}$, is composed to approximately equal parts of a direct $\omega \to 3\pi$ and a $\omega \to \rho\pi$ coupling, represented by anomalous terms in the interaction Lagrangian,

$$\mathcal{L}_{\omega\rho\pi} = G_{\omega\rho\pi}\, \epsilon_{\mu\nu\sigma\tau}\, \omega^\mu\, \partial^\nu \vec{\rho}^{\,\sigma} \cdot \partial^\tau \vec{\pi}\,, \tag{7}$$

$$\mathcal{L}_{\omega 3\pi} = G_{\omega 3\pi}\, \epsilon_{\mu\nu\sigma\tau}\, \omega^\mu\, (\partial^\nu \vec{\pi} \times \partial^\sigma \vec{\pi}) \cdot \partial^\tau \vec{\pi}\,. \tag{8}$$

With a hadronic formfactor cutoff-parameter, $\Lambda_{\omega\rho\pi} = 1$ GeV, and using the VDM [45], one finds for the radiative decay width $\Gamma_{\omega\to\pi\gamma} = 0.72$ MeV which approximately agrees with the updated experimental value of 0.76 ± 0.03 MeV [52].

In cold nuclear matter, the renormalization of the π-ρ cloud has been found to be rather sensitive to the medium effects on the ρ [38, 48, 53, 54], which is due to the fact that the $\omega \to \pi\rho(\to \pi\pi\pi)$ decay proceeds via the low-mass tail of the ρ-spectral function below its nominal mass of 770 MeV. In Ref. [53] 80% of the estimated in-medium broadening at nuclear saturation density is attributed to the in-medium ρ spectral function (taken from Ref. [33]), resulting in $\Gamma_{\omega P}(\varrho_0) \simeq 60$ MeV. Likewise, a large contribution to second order in the nuclear density, $\mathcal{O}(\varrho_N^2)$, to $\Gamma_{\omega P}(\varrho_N)$ arises due to the simultaneous dressing of both π and ρ [54]. Following Ref. [38], we restrict ourselves to the impact of the in-medium ρ by folding the phase space in the $\omega \to \pi\rho$-decay width over the spectral function evaluated in the previous section,

$$\Gamma_{\omega\to\rho\pi}(s) = \frac{2G_{\omega\rho\pi}^2}{8\pi} \int_0^{M_{\rm max}} \frac{M{\rm d}M}{\pi}\, A_\rho(M)\, 2q_{\rm cm}^3 \times [1 + f^\pi(\omega_\pi) + f^\rho(E_\rho)]\, F_{\omega\rho\pi}(q_{\rm cm})^2\,, \tag{9}$$

where $M_{\rm max}=\sqrt{s}-m_\pi$, $\omega_\pi^2 = m_\pi^2 + q_{\rm cm}^2$, $E_\rho^2 = M^2 + q_{\rm cm}^2$, and $q_{\rm cm}$ is the three-momentum of π and ρ in the rest frame of the ω. In addition we account for cold-nuclear matter effects due to the two most important direct ω-N excitations, $\omega N(1520)N^{-1}$ and $\omega N(1650)N^{-1}$, as identified in Ref. [55] in a coupled-channel analysis of empirical vector-meson nucleon scattering amplitudes. Recent measurements of $\pi^0\gamma$-invariant mass spectra in photon-induced production off hydrogen and Nb targets have revealed a low-mass shoulder [56] that has been interpreted as reduced ω mass in nuclear matter. However, this interpretation is not free of controversy and may also be explained by a large increase of the ω width to about 90 MeV [57]. The latter is compatible with the ω propagator employed in the present paper.

Finite-temperature effects on the ω propagator include Bose-enhancement factors in the π-ρ cloud, the in-medium ρ propagator in Eq. (9), a schematic estimate of the inelastic $\pi\omega \to \pi\pi$ width based on Ref. [58], and a full calculation of the thermal $\omega+\pi \to b_1(1235)$ loop [38].

The predicted average ω width in the hadronic phase of URHICs is $\Gamma_\omega^{\rm med} \simeq 100$ MeV [12], cf. middle panel of Fig. 2, quite consistent with the results of Ref. [59]. This has the interesting consequence [38] that if dilepton spectra

in HICs show a structure of ∼100 MeV width in the ρ-/ω mass region, it would be an unambiguous signature of the in-medium ω spectral function since it is narrower than the lower limit given by a free ρ contribution, $\Gamma_\omega^{\rm med} < \Gamma_\rho^{\rm vac} \simeq 150$ MeV.

3. ϕ Meson

For the ϕ, collision rates in a meson gas have been estimated to amount to a broadening by $\sim$ 20 MeV at $T = 150$ MeV [60]. The dressing of the kaon cloud is presumably the main effect for ϕ modifications in nuclear matter, increasing its width by $\sim$ 25 MeV at saturation density [61]. Recent data on ϕ absorption in nuclear photoproduction suggest substantially larger values [62]. Since a quantitative, empirically constrained treatment of the ϕ in hot and dense matter is not available at present, we will consider the ϕ width as a parameter. Following Ref. [15] we augment the microscopic calculations of Ref. [38] by a factor of 4 to roughly agree with the phenomenological values extracted from nuclear photoproduction [62]. The corresponding ϕ spectral functions under SPS conditions are displayed in the lower panel of Fig. 2. The average width over the fireball evolution amounts to $\Gamma_\phi^{\rm med} \simeq 80$ MeV.

C. Hadronic Emission at Intermediate Mass: Multi-Pion Annihilation

Above the ϕ mass, the hadronic structure of the (vacuum) e.m. correlator becomes more involved being characterized by overlapping broad resonances which combine into continuum-like multi-meson states (most notably isovector four-pion states), recall Fig. 1. To estimate medium effects in this regime, we take recourse to model-independent predictions following from a low-temperature expansion evaluated using chiral-reduction techniques for the corresponding matrix elements involving thermal pions. This method has been first worked out in Ref. [63] in the chiral limit ($m_\pi = 0$) and leads to the chiral mixing formula for the isovector part of vector and axialvector correlators,

$$\begin{aligned} \Pi_V(q) &= (1-\varepsilon)\,\Pi_V^{\rm vac}(q) + \varepsilon\,\Pi_A^{\rm vac}(q)\,, \\ \Pi_A(q) &= \varepsilon\,\Pi_V^{\rm vac}(q) + (1-\varepsilon)\,\Pi_A^{\rm vac}(q)\,. \end{aligned} \tag{10}$$

The mixing coefficient ε is determined by pion tadpole diagrams via a loop integral

$$\varepsilon = \frac{2}{f_\pi^2}\int \frac{d^3k}{(2\pi)^3\omega_k^\pi}\; f^\pi(\omega_k^\pi;T) \tag{11}$$

(ω_k^π: on-shell pion energy, $f_\pi = 93$ MeV: pion decay constant). For $\varepsilon \to 1/2$, V and A correlators degenerate signaling chiral-symmetry restoration (at $T_c^{\rm mix}\simeq$160 MeV). Note that the admixture of the axialvector part in the $M = $ 1-1.5 GeV region (which corresponds to the a_1 resonance) fills in the "dip" structure of the vector correlator (recall Fig. 1); for $\varepsilon \to 1/2$ both spectral functions merge into the perturbative-QCD continuum for $M \geq 1$ GeV which has been interpreted [1] as a lowering of the quark-hadron duality scale, $M_{\rm dual}$, cf. Eq. (4). The simple form of Eq. (10) only holds in the soft-pion limit, *i.e.*, when neglecting the pion four-momenta in $\Pi_{V,A}$. More elaborate treatments [64, 65] will broaden and somewhat reduce the enhancement in the $M \simeq$ 1-1.5 GeV region [66]. We here implement the mixing effect on the (isovector) four-pion part utilizing Eq. (10) with a mixing parameter $\hat\varepsilon = \frac{1}{2}\varepsilon(T,\mu_\pi)/\varepsilon(T_c,0)$ with finite pion mass ($m_\pi = 139.6$ MeV), critical temperature, T_c, and pion chemical potentials ($\mu_\pi > 0$) implemented as an overall fugacity factor, $z_\pi = {\rm e}^{\mu_\pi/T}$, in Boltzmann approximation (μ_π varies according to the thermal fireball evolution discussed in Sec. IV below). The two-pion piece, as well as the three-pion piece corresponding to a_1 decay, $a_1 \to \pi + \rho$, have been removed as they are included via the ρ-spectral function as discussed above. A detailed analysis of the derivation of Eq. (10) in the presence of a finite pion-chemical potential leads to the following expression for the mixing effect on the vector-isovector current correlation function:

$$\Pi_V(q) = (1-\hat\varepsilon) z_\pi^4 \Pi_{V,4\pi}^{\rm vac} + \frac{\hat\varepsilon}{2} z_\pi^3 \Pi_{A,3\pi}^{\rm vac} + \frac{\hat\varepsilon}{2}(z_\pi^4 + z_\pi^5)\Pi_{A,5\pi}^{\rm vac}\,. \tag{12}$$

D. Hadronic Emission at High Momentum: Meson t-Channel Exchange

As discussed in the Introduction, a current discrepancy in the theoretical description of the NA60 data concerns the dilepton yield at high transverse pair-momentum, $q_T > 1$ GeV, for masses $M \leq 1$ GeV. It is therefore important to scrutinize the vector-meson spectral function calculations for high momentum sources. The latter are typically associated with t-channel meson exchanges, rather than s-channel resonances whose decay products are suppressed at momenta far off the resonance. In the spectral-function approach, t-channel exchange processes are encoded in medium modifications of the pseudoscalar meson cloud. As elaborated in Sec. II B 1, the pion-cloud modifications of the ρ explicitly include interactions with baryons, but not with thermal mesons. Consequently, t-channel meson exchanges are present for ρB interactions, but not for $\rho\pi$. E.g., the experimental $\pi N \to \rho N$ cross section is properly reproduced at large $\sqrt{s}$ where t-channel π exchange dominates. Indeed, it has been found in Ref. [11] in the context of thermal photon production that t-channel exchanges in $\rho + \pi \to \pi + \gamma$ outshine the contributions from the ρ-spectral function at momenta above ∼1 GeV for $T = 200$ MeV (at smaller temperatures the importance of t-channel exchanges is reduced). Most notably, ω exchange emerged as the single most important hadronic high-q_T thermal photon source.

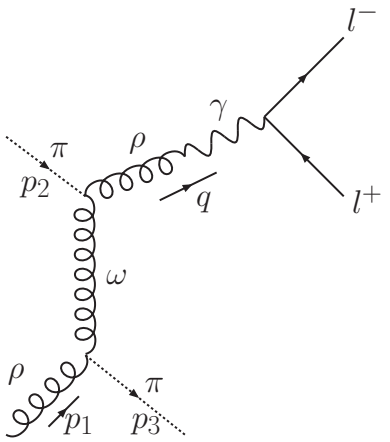

FIG. 3: The Feynman diagram corresponding to the annihilation of a ρ meson via ω-meson exchange in the t channel.

To estimate the relevance of t-channel exchanges in $\pi\rho$ scattering for thermal dileptons, we adopt the same simplified treatment as in Ref. [11], properly extended to a finite invariant mass of the virtual photon (lepton pair): rather than implementing the pertinent diagram into the ρ selfenergy, we employ the standard kinetic theory expression for the thermal production rate

$$\frac{\mathrm{d}N^{(\text{t-ch})}_{\pi\rho\to\pi ll}}{\mathrm{d}^4x\mathrm{d}^4q} = \int\frac{\mathrm{d}^3p_1}{2\omega^\rho_{p_1}(2\pi)^3}\int\frac{\mathrm{d}^3p_2}{2\omega^\pi_{p_2}(2\pi)^3}\int\frac{\mathrm{d}^3p_3}{2\omega^\pi_{p_3}(2\pi)^3} \times(2\pi)^4\delta^{(4)}(p_1+p_2-p_3-q)\sum|\mathcal{M}_{\pi\rho\to\pi ll}|^2 \times[1+z_\pi f^B(\omega^\pi_{p_3};T)]\frac{z_\pi^3 f^B(\omega^\rho_{p_1};T)f^B(\omega^\pi_{p_2};T)}{4(2\pi)^6}\,, \tag{13}$$

which allows to calculate the contribution for $\pi+\rho\to\pi+l^++l^-$ in terms of the corresponding matrix element, $\mathcal{M}_{\pi\rho\to\pi ll}$, in Born approximation. The latter substantially facilitates the task of maintaining gauge invariance. For the $\rho\omega\pi$ vertex, the anomalous-coupling Lagrangian, Eq. (7), is used to calculate the matrix element,

$$\begin{aligned}\sum|\mathcal{M}_{\omega\mathrm{t}}|^2 =&\frac{4\pi^2\alpha g^4_{\rho\omega\pi}C^2}{M^2}(m_\rho^{(0)})^4|D_\rho(M)|^2\frac{1}{|t-m_\omega^2|^2}L(M)\Theta(M-2m_l)\\ &\times\{(M^2-m_\pi^2)^2(m_\pi^2-m_\rho^2)^2-2t[m_\pi^2(M^2-m_\rho^2)^2+(M^2-m_\pi^2)(m_\rho^2-m_\pi^2)s]\\ &+t^2[(M^2+2m_\pi^2+m_\rho^2)^2-2(M^2+2m_\pi^2+m_\rho^2)s+2s^2]-2t^3(M^2+2m_\pi^2+m_\rho^2-s)+t^4\}\,,\end{aligned} \tag{14}$$

corresponding to the Feynman diagram depicted in Fig. 3; M denotes the invariant mass of the lepton pair; $s=(p_1+p_2)^\mu(p_1+p_2)_\mu$ and $t=k^\mu k_\mu$ are the usual Mandelstam variables with $k^\mu=(p_3-p_1)^\mu$ the exchanged four-momentum. The ρ-γ vertex has been written in the form [45]

$$\mathcal{L}_{\rho\gamma}=-Cm_\rho^2A_\mu\rho^\mu \tag{15}$$

where $C=e/g_\rho=0.052$. Medium effects on the ρ meson are implemented by using the full in-medium propagator, $D_\rho(M)$, for the intermediate ρ meson which couples to the photon (upper ρ line in Fig. 3, with $M^2=q^2$) and by folding Eq. (14) over the in-medium spectral function for the incoming ρ (lower ρ line in Fig. 3, with $m_\rho^2=p_1^2$ and a weight $-2m_\rho/\pi\,\mathrm{Im}\,D_\rho(m_\rho)$). To avoid double counting with the ω s-channel graph already included in the in-medium ρ-selfenergy, the integral in Eq. (13) is restricted to spacelike ω-exchange momenta, *i.e.*, $t<0$. The coupling constant, $g_{\rho\omega\pi}=25.8\ \mathrm{GeV}^{-1}$, has been fixed in [45] by a simultaneous fit to the hadronic and radiative ω decays including a hadronic dipole-form factor,

$$F(t)=\left(\frac{2\Lambda^2}{2\Lambda^2-t}\right)^2, \tag{16}$$

with $\Lambda=1$ GeV. To maintain gauge invariance in a simplified way as in Ref. [11], we pull the formfactor outside the integral and introduce an average momentum transfer, $\bar{t}$ (adapted to the finite mass of the virtual photon), according to

$$\frac{F^4(\bar{t})}{(m_\omega^2-\bar{t})^2}=\frac{1}{2}\int_{-1}^{1}\mathrm{d}x\frac{F^4[t(x)]}{[m_\omega^2-t(x)]^2}\,, \tag{17}$$

$$t(x)=M^2+m_\pi^2-2(M^2+q^2-qpx)\,. \tag{18}$$

The amplitude, Eq. (14), is then multiplied by $F^4(\bar{t})$. Eq. (13) furthermore accounts for pion fugacity factors, z_π due to finite pion chemical potentials, implemented in Boltzmann approximation (*e.g.*, for the incoming π and ρ this amounts to a total fugacity of z_π^3). In Fig. 4 we summarize our results for the ω t-channel emission rate, integrated over three-momentum, for conditions along our default trajectory for In(158 AGeV)+In collisions at SPS (including finite μ_π). The upper panel illustrates that the implementation of the in-medium ρ propagator (which was not done in Ref. [11]) leads to a notable reduction in the emission rate, which is mostly due to the reduction in the intermediate ρ propagator, $|D_\rho(M)|^2$. We have verified that medium effects on the ω propagator are negligible (in the spacelike regime finite-width effects are insignificant as long as $\Gamma_\omega\ll m_\omega$). In the middle panel,

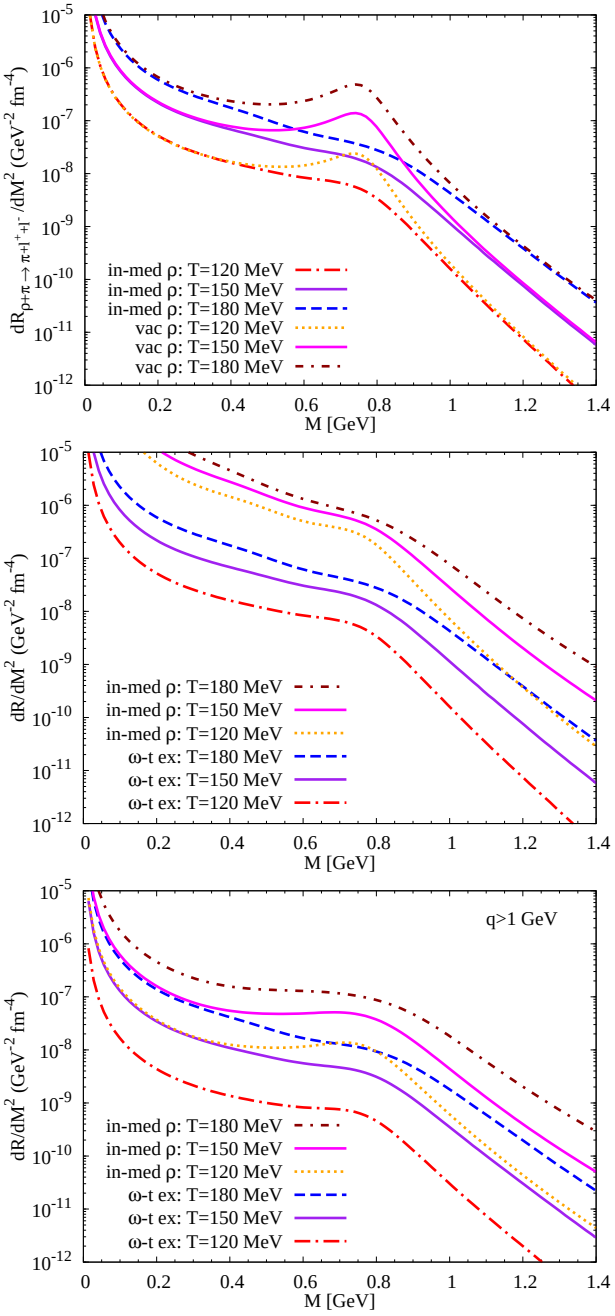

FIG. 4: Three-momentum integrated thermal emission rates from ω t-channel exchange in the $\pi\rho \to \pi e^+e^-$ reaction. Upper panel: comparison of the rates when using either the free or the in-medium ρ propagators in both the matrix element and the incoming ρ-mass distribution. Middle panel: comparison of the in-medium ω t-channel rates with thermal rates from the full in-medium ρ spectral function. Lower panel: same as middle panel, but restricting the momentum integration to $q > 1$ GeV. All curves for T=150 MeV and 120 MeV include pertinent pion fugacities at $\mu_\pi = 39$ MeV and 79 MeV, respectively.

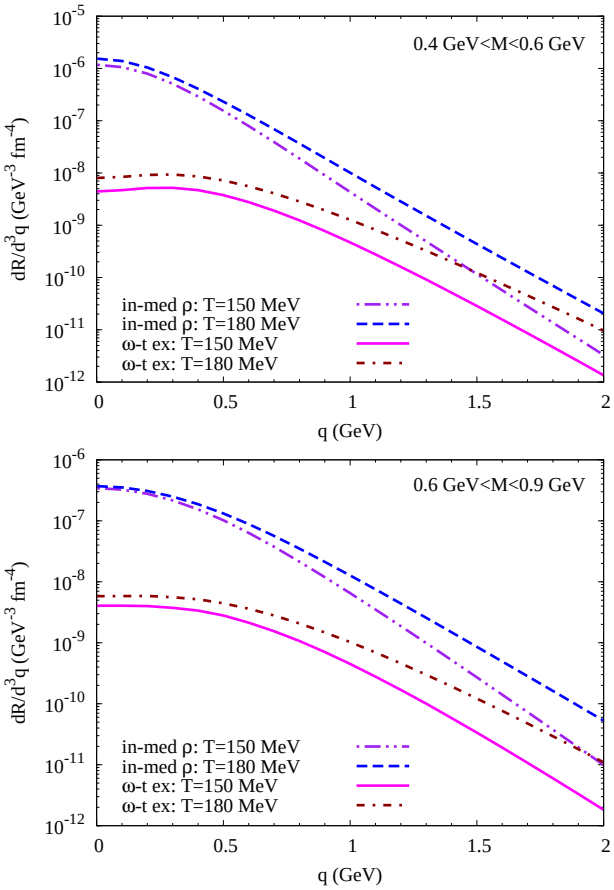

FIG. 5: Mass-integrated dilepton rates as a function of three-momentum for ω t-channel exchange in $\pi\rho \to \pi e^+e^-$ (computed with in-medium ρ propagators) and the leading contribution from the full in-medium-ρ spectral function. As in Fig. 4, the results for T=150 MeV include pion fugacity factors.

the comparison of the in-medium ω t-channel rates to the ones from the full in-medium ρ spectral function [24], based on Eq. (1), confirms that the former contribution is indeed small in magnitude. However, if one applies a three-momentum cut of $q > 1$ GeV (lower panel), the relative magnitude of the t-channel contribution increases, as anticipated at the beginning of this section. But even in this case the relative strength of the ω t-channel exchange is rather moderate. The increasing contribution at higher momentum can be more directly seen when integrating the rate, Eq. (13), over invariant mass bins and plotting it versus q, cf. Fig. 5.

As indicated above, in our calculations of dilepton spectra in Sec. V, we will implement the ω t-channel emission rate, Eq. (13), by an incoherent addition to the main contribution, Eq. (1). This neglects interference terms in the pertinent selfenergy contribution in the (denominator of the) ρ spectral function, which is justified due to the relative smallness of the ω t-channel part. To simulate the presence of other t-channel processes (*e.g.*, π and a_1 exchange), guided by the photon rate calculations of Ref. [11], we will multiply the ω t-channel contribution by a factor of 2 in our calculation of dilepton spectra

below.

E. Partonic Emission: Quark-Antiquark Annihilation

Emission from the QGP is calculated using the hard-thermal-loop improved rate for $q\bar{q}$ annihilation [67], including an extrapolation to finite three-momentum. It turns out [68] that this rate has the conceptually attractive feature that it closely coincides with the rate in hadronic matter when both are extrapolated to the expected phase-transition region. This is suggestive for a kind of quark-hadron duality [24] and has the additional benefit that the emission from the expanding fireball can be anticipated to become rather insensitive to details of how the phase transition is implemented (*e.g.*, to the values for the critical temperature or "latent heat"). This point will be studied explicitly in Sec. V C below.

Recent (experimental and theoretical) developments suggest that the QGP features significant nonperturbative effects for temperatures up to $\sim$1.5-2T_c, *e.g.*, the survival of (hadronic) resonances and/or bound states, even in the light-quark sector. Possible consequences for the dilepton emission rate have been estimated in Ref. [69]. Depending on the width of these states, a maximal enhancement of up to a factor of ~ 2 over the perturbative QGP emission rate at intermediate masses (*i.e.*, in the mass range of 1.5-2 GeV) is conceivable. We will not further pursue this possibility in the present paper.

III. DILEPTON SOURCES OTHER THAN THERMAL RADIATION

In this section we address dilepton sources other than radiation from a thermal source as given by Eq. (1), *i.e.*, ρ decays after thermal freezeout, decays of primordially produced ρ mesons which escape the fireball, and primordial Drell-Yan annihilation. For simplicity, we generically refer to these sources as "non-thermal", even though the freezeout decays, *e.g.*, are represented by thermal "blast-wave" spectra commonly used to characterize light hadron spectra in heavy-ion collisions.

A. ρ Mesons at Thermal Freezeout

Dilepton decays of long-lived hadrons (most notably Dalitz decays of η and ω, as well as exclusive l^+l^- decays of ω and ϕ) can be rather well separated from the freezeout of the interacting fireball in heavy-ion collisions, which has given rise to the notion of the "hadronic decay cocktail" contribution to dilepton spectra, computed using the free spectral shape of the decaying mesons. For the ρ meson, due to its short lifetime, such a separation is not well defined. Therefore, when adding thermal radiation to the cocktail, the ρ is commonly removed from the latter and implemented into the thermal yield. In previous works [15, 24, 36] this was done by running the fireball an extra $\sim$1 fm/c using the in-medium ρ spectral function. It turns out [19, 20], however, that this description of ρ decays at thermal freezeout carries an extra factor of $1/\gamma$ relative to a standard blast-wave spectrum of hadrons at thermal freezeout, where $\gamma = q_0/M$ is the usual Lorentz factor. Roughly speaking, the in-medium radiation given by Eq. (1) is proportional to the electromagnetic decay width times the fireball lifetime, $(\Gamma_{ll}/\gamma)\tau_{\rm FB}$, while decays after freezeout are proportional to the branching ratio of electromagnetic to total lifetime, $\Gamma_{ll}/\Gamma_\rho^{\rm fo}$, where the γ factor cancels (as usual, we define Γ_X as the partial decay width in the rest system of the particle). The remainder of this section will give a more detailed discussion of this.

To account for the correct time dilation effects in the calculation of dilepton decays of ρ-mesons after thermal freezeout, we use the standard Cooper-Frye description [70],

$$\mathrm{d}N = q_\mu \mathrm{d}\sigma^\mu \frac{\mathrm{d}^3q}{(2\pi)^3 q^0} f_B\left(\frac{q_\nu u^\nu}{T}\right), \tag{19}$$

for the phase-space distribution of an on-shell particle ($q_\mu q^\mu{=}m^2$) at thermal freezeout; T and $u^\nu = \gamma(1,\beta_\perp)$ denote the local temperature and four velocity (flow) of the fluid cells of the medium, and $\mathrm{d}\sigma^\mu$ is the hypersurface normal vector defined by an appropriate freezeout condition. In accordance with the homogeneous fireball model described in Sec. IV, thermal freezeout at a constant time $t = x^0$ in the laboratory frame is assumed, *i.e.*, $(\mathrm{d}\sigma^\mu) \equiv (\mathrm{d}^3x, 0, 0, 0)$. The in-medium ρ spectral function at freezeout is introduced via the substitution

$$\frac{\mathrm{d}^3q}{q_0} \to \mathrm{d}^4q\; 2\delta^+(q_\mu q^\mu - m^2) \to \mathrm{d}^4q \frac{A_\rho}{\pi}\;, \tag{20}$$

where $A_\rho = -2/3\,\mathrm{Im}(D_\rho)^\mu_\mu$ (as before) includes the average over the three polarizations via the Lorentz trace which runs over the physical (*i.e.*, four-momentum transverse) components of the propagator. To properly treat the low-mass tails of the spectral function, one would have to resolve the individual resonance decays figuring into the ρ selfenergy. To simplify our task, we circumvent this problem by employing the vacuum form of the ρ selfenergy augmented with a width corresponding to the full-width-half-maximum of the in-medium spectral function at thermal freezeout ($\Gamma_\rho^{\rm fo} \simeq 260$ MeV). The distribution of ρ mesons at thermal freezeout then reads

$$\frac{\mathrm{d}N_\rho^{\rm fo}}{\mathrm{d}^3x\mathrm{d}^4p} = p^0 \frac{3A_\rho}{8\pi^4} f^B\left(\frac{p_\nu u^\nu}{T}\right)\;. \tag{21}$$

In accordance with the averaging procedure over the freezeout duration, we evaluate the transverse four-velocity for the freezeout ρ at a time $\Delta\tau_\rho^{\rm fo}/2 \simeq 0.5$ fm/c after the thermal emission, Eq.(1), has shut off. The dilepton rate follows by folding with the appropriate partial decay width. Within our vector-meson dominance

model this is given by the matrix element for the process $\rho \to \gamma^* \to l^+ + l^-$, and after integration over $t \in (t_{\rm fo}, \infty)$ this results in

$$\begin{aligned}\frac{\mathrm{d}N_{ll}^{(\rm fo)}}{\mathrm{d}^3x\mathrm{d}^4q} &= \frac{q^0}{M}\,\frac{\alpha^2 m_\rho^4}{g_\rho^2 M^2}\frac{A_\rho}{2\pi^3}L(M)f^B\left(\frac{p_\nu u^\nu}{T}\right)\frac{1}{\Gamma_\rho^{\rm fo}} \\ &= \frac{q_0}{M}\frac{1}{\Gamma_\rho^{\rm fo}}\left(\frac{\mathrm{d}N_{ll}}{\mathrm{d}^4x\mathrm{d}^4q}\right)_{t=t_{\rm fo}}, \end{aligned} \tag{22}$$

where L is the dilepton-phase space factor (3). The second line of Eq. (22) shows that the momentum dependence of the dilepton distribution from ρ decays after thermal freeze-out deviates from the rate from a thermal source (1) by a Lorentz factor $\gamma \equiv q_0/M = \sqrt{M^2+q^2}/M$. The physical origin of this difference is the time dilation of the total lifetime of a freeze-out ρ meson with three-momentum q which is absent in the formula for radiation from a thermal source, because its ρ-meson abundance at each instant of time is fixed by the temperature and pion-chemical potential of the medium (as required by detailed balance of ρ formation and decay), and thus the total number of thermal dileptons is determined by the lifetime of the fireball. Note, however, that the thermal rate is proportional to Γ_{ll} with an associated time dilation factor $1/\gamma$. The freezeout-ρ dilepton spectra are thus equivalent to standard blast-wave descriptions of stable hadrons [85].

Our default assumption for the radial profile of the flow field is a linear dependence on the radius according to

$$\beta_\perp(r,t) = \beta_\perp^s \frac{r}{R(t)}, \tag{23}$$

where $R(t) = r_0 + a_\perp t^2/2$ is the radius of the fire-cylinder, $\beta_\perp^s = a_\perp t$ its surface speed, and $r \le R(t)$ the radial coordinate of the fluid cell related to the volume element $\mathrm{d}^3x = 2\pi r\mathrm{d}r\mathrm{d}z$ (since we neither address azimuthal asymmetries nor peripheral collisions in this work, we approximate the cross sectional area of the fire cylinder as a circle).

B. Primordial ρ Mesons

Another source of non-thermal dileptons is the decay of ρ mesons which originate from primordial hard-scattering processes and traverse the interaction zone without equilibrating. We evaluate this contribution within a schematic jet-quenching model [20], as follows.

First, we construct the q_T spectrum of primordial ρ mesons assuming a power law,

$$\frac{1}{q_T}\frac{\mathrm{d}N_{\rm prim}}{\mathrm{d}q_T} = \frac{A}{(1+Bq_T^2)^a}\ , \tag{24}$$

with parameters estimated from p-p scattering data [71], $B = 0.525\mathrm{GeV}^{-2}$ and $a = 5.5$. The total number of primordial ρ's in A-A collision is determined based on the empirical freezeout systematics of light hadron production, *i.e.*, we calculate the expected total number of ρ mesons in In-In at $T_c = 175$ MeV and match the norm of the primordial spectrum, Eq. (24), to it. At the same time, we have to take care of the correct scaling properties of the spectrum at high momentum: while the (total) yield at low q_T is proportional to the number of participant nucleons, the high-q_T yield should scale with the number of primordial N-N collisions. We implement this transition by a continuous linear switching between the two regimes over the range 1 GeV $< q_T <$ 3 GeV.

Second, we implement a Cronin effect for A-A collisions by a "Gaussian smearing" of Eq. (24),

$$\frac{\mathrm{d}N_{\rm prim}^{\rm cron}}{\mathrm{d}^2q_T} = \int \frac{\mathrm{d}^2k_T}{\pi\Delta k_T^2}\frac{\mathrm{d}N_{\rm prim}}{\mathrm{d}^2k_T}\exp\left[-\frac{(q_T-k_T)^2}{\Delta k_T^2}\right], \tag{25}$$

with a conservative estimate of $\Delta k_T^2 = 0.2$ GeV^2 as extracted in Ref. [11] based on direct photon spectra in p-A reactions.

Third, we calculate a suppression factor representing the probability for primordial ρ mesons to escape the medium without rescattering, using Monte Carlo techniques. In line with our fireball model, we start from a spatially homogeneous distribution in the transverse plane at the QGP formation time. The escape probability for a ρ with momentum q is then calculated as

$$P = \exp\left(-\int \mathrm{d}t\ \sigma_\rho^{\rm abs}(t)\ \varrho(t)\right), \tag{26}$$

where the absorption cross section

$$\sigma_\rho^{\rm abs}(t) = \begin{cases}\sigma_{\rm ph} = 0.4\ \mathrm{mb} & \text{for} \quad t < q_0/m_\rho\,\tau_{\rm f} \\ \sigma_{\rm had} = 5\ \mathrm{mb} & \text{for} \quad t > q_0/m_\rho\,\tau_{\rm f}\end{cases} \tag{27}$$

depends on the ρ-meson formation time in its rest frame, which is assumed to be $\tau_{\rm f}$=1 fm, augmented by Lorentz time dilation in the fireball frame; $\sigma_{\rm ph}$ and $\sigma_{\rm had}$ denote the pre-hadronic and hadronic absorption cross sections of the ρ, respectively, and $\varrho(t)$ the corresponding particle density of the fireball medium (partonic or hadronic; if the ρ meson has not formed by the time the system has hadronized, we use constituent quark scaling to infer the partonic density as $\varrho_{\rm p} = 3\varrho_{\rm had}$, and vice versa).

A rough check of our construction may be obtained by comparing the ρ spectra to measured pion spectra in A-A collisions at the SPS. Since pion spectra contain both a hard (primordial) and a soft (thermal + flow) component, a comparison with our ρ spectra should contain both the primordial part constructed in this section and the thermal freezeout contribution described in the previous section, III A. We do this comparison in terms of the nuclear modification factor, R_{AA}, defined as the ratio of the spectrum in A-A collisions over the collision-number scaled spectrum in p-p. The upper panel of Fig. 6 shows that the jet-quenching + freezeout-ρ model results in fair agreement with a recent compilation of R_{AA} for pions in S-Au and Pb-Pb systems from various experiments at full SPS

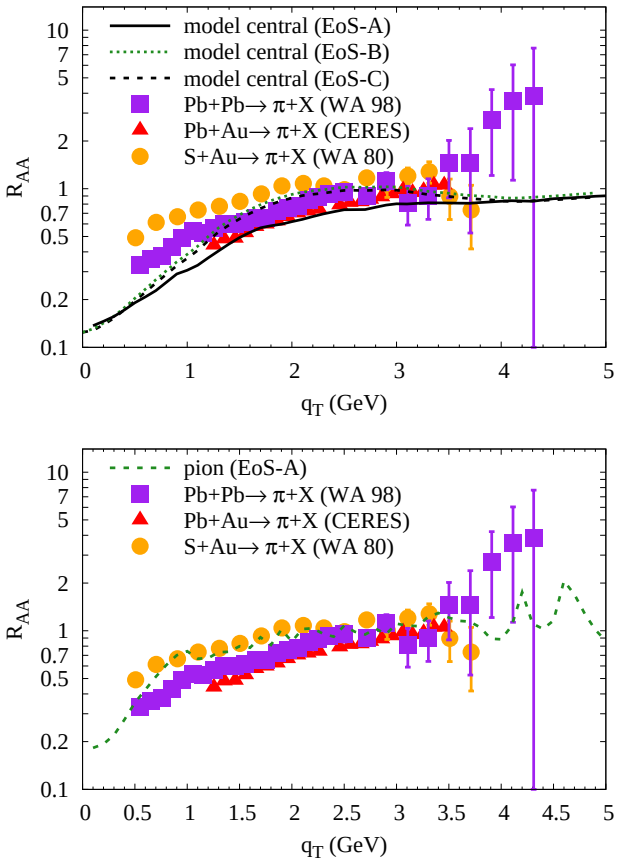

FIG. 6: (Color online) Nuclear modification factor for transverse momentum spectra of ρ (upper panel) and π mesons (lower panel) from primordial (hard) production plus thermal freezeout, compared to a compilation of data for R_{AA} of pions at full SPS energy [72] for central collisions with the standard equation of state (EoS-A, full line) and an EoS with $T_{\rm ch} = 160$ MeV (EoS-B+C as discussed in Sec. IV, dashed line). The primordial ρ spectra include effects of initial Cronin smearing and jet-quenching in the expanding fireball, while the thermal freezeout ρ's are taken from Sec. III A (same for the pions, but without finite-width effects).

energy [72]. As a check of this procedure, as well as of the fireball model, we plot in the lower panel of Fig. 6 the calculated pion R_{AA} for central In-In at SPS (as a sum of the jet-quenching plus thermal-freezeout components) for central In-In at SPS; the agreement with data is reasonable (note that resonance decays are not included, which are mostly concentrated at low q_T).

C. Drell-Yan Annihilation and Correlated Charm Decays

In the high-mass region (HMR, $M > 3$ GeV), dilepton spectra in nuclear collisions are expected to be dominated by the Drell-Yan (DY) process, *i.e.*, primordial annihilation of quarks and antiquarks within the incoming nucleons. To leading order, this process does not depend on the strong coupling constant (it is purely electromagnetic, $\mathcal{O}(\alpha_s^0\alpha_{\rm em}^2)$) and can therefore be rather reliably evaluated, provided one has a good knowledge of the parton-distribution functions (PDFs) within the nucleon. In a central collision ($b = 0$) of two equal nuclei with mass number A, the invariant-mass spectrum of Drell-Yan pairs per unit rapidity is given by

$$\left.\frac{{\rm d}N_{\rm DY}^{AA}}{{\rm d}M{\rm d}y}\right|_{b=0} = \frac{3}{4\pi R_0^2}\, A^{4/3}\, \frac{{\rm d}\sigma_{\rm DY}^{NN}}{{\rm d}M{\rm d}y} \tag{28}$$

in terms of the standard DY cross section in an elementary nucleon-nucleon (N-N) collision,

$$\frac{{\rm d}\sigma_{\rm DY}^{NN}}{{\rm d}M{\rm d}y} = K\frac{8\pi\alpha}{9sM}\sum_{q=u,d,s} e_q^2\left[q(x_1)\bar{q}(x_2) + \bar{q}(x_1)q(x_2)\right] \ . \tag{29}$$

Here, $q(x_{1,2})$ and $\bar{q}(x_{1,2})$ denote the (collinear) quark and anti-quark distribution functions, respectively (neglecting nuclear effects). Their arguments are related to the center-of-mass (cms) rapidity, y, and the invariant mass of the lepton pair as $x_{1,2} = xe^{\pm y}$ with $x = M/\sqrt{s}$, where $\sqrt{s}$ is the cms energy of the N-N collision. The root-mean-squared radius parameter in Eq. (28), $R_0 \simeq 1.05$ fm, arises from a folding over a Gaussian thickness function; for simplicity, we will adopt Eq. (28) also for non-central collisions with an accordingly reduced number of participants, A. For the parton distribution functions we employ the leading-order parameterization from Ref. [73] (GRV94LO), which incorporate isospin asymmetries in the sea-quark distributions which significantly reduce the need for additional isospin corrections for nuclei with $N \neq Z$ (*e.g.*, less than 5% for Pb-Pb collisions), which will be neglected here [74]. In Eq. (29) higher-order corrections in α_s are encoded in an empirical K factor, which turns out to be $K \simeq 1.5$ to reproduce DY production in p-A collisions [74].

In addition to generating a K factor, higher-order effects manifest themselves in a nonzero pair-q_T of the DY dileptons. To obtain a realistic q_T spectrum, we follow the procedure adopted by the NA50 collaboration [7, 8]: based on a comprehensive analysis of p-A and A-A collisions at the SPS it has been found that the IMR and HMR dilepton spectra can be fairly well described by assuming a Gaussian shape for the DY spectrum,

$$\frac{{\rm d}N_{\rm DY}}{{\rm d}M{\rm d}y{\rm d}q_T^2} = \frac{{\rm d}N_{\rm DY}}{{\rm d}M{\rm d}y}\,\frac{\exp(-q_T^2/2\sigma_{q_T}^2)}{2\sigma_{q_T}^2} \tag{30}$$

with $\sigma_{q_T} \simeq 0.8 - 1$ GeV. In Ref. [9], a value of $\sigma_{q_T} \simeq 0.8$ GeV has resulted in reasonable agreement with the NA50 q_T spectra for IMR dimuons in central Pb-Pb; for $\sigma_{q_T} \simeq 0.9$ GeV, which increases the spectrum at $q_T = 2$ GeV by 50%, the agreement with NA50 would still be acceptable. Here, we adopt $\sigma_{q_T} \simeq 0.8$ GeV providing a conservative estimate of the DY contribution.

The extrapolation of the DY spectrum to the regions where both mass and momentum are small (say, below

$M, q_T \simeq 1.5$ GeV) is problematic, but fortunately its contribution in this regime is small compared to, *e.g.*, thermal emission in A-A collisions. There is, however, an additional constraint provided by the photon point ($M \to 0$) which allows to extrapolate the DY spectra to low mass, at least for reasonably large momenta, $q_T > 1$ GeV (which is the regime were the DY yield is noticeable). Formally, the photon-production rate follows from the dilepton one by taking the limit $M \to 0$. More specifically, this is encoded in the relation

$$q_0 \frac{\mathrm{d}R_\gamma}{\mathrm{d}^3 q} = -\frac{\alpha}{2\pi^2} \, \mathrm{Im}\, \Pi^\mu_{\mathrm{em},\mu}(M=0,q) f^B(q_0;T) \qquad (31)$$

with the same e.m. current-current correlation function, $\Pi^{\mu\nu}_{\mathrm{em}}$ of Eq. (2), as in the dilepton rate, Eq. (1). For $q \gg M$, the M-dependence of Π_{em} is weak, and the difference between $q_0 \frac{dN_{ll}}{dM d^3q}$ and $q_0 \frac{\mathrm{d}R_\gamma}{\mathrm{d}^3 q}$ amounts to a factor of $\frac{2\alpha}{3\pi M}$. Thus we can evaluate the DY q_T spectrum at a mass M_{cut} and extrapolate it down in mass to the photon point using the factor M_{cut}/M. For M_{cut}=0.8-1 GeV, in connection with $\sigma_{q_T} \simeq 0.8$ GeV, reasonable agreement with the primordial photon spectrum of Ref. [11] is found.

In addition, there could be "pre-equilibrium" contributions from secondary Drell-Yan processes [74] (*e.g.*, $\pi N \to \mu\mu X$ involving primordially produced pions), which turn out to be rather sensitive to the pion formation time. *E.g.*, for $\tau^\pi_{\mathrm{form}} = 1$ fm/c, the enhancement over primordial Drell-Yan annihilation in central S-U was found to be ∼10% at $M = 2$ GeV. In a thermal emission description, which we employ here after a rather early thermalization time of $\tau_0 = 1$ fm/c, it is difficult to separate pre-equilibrium radiation from thermal emission (e.g., secondary Drell-Yan in π-N interactions might overlap with thermal q-$\bar{q}$ annihilation). A rough estimate of pre-equilibrium effects may be obtained by varying the thermalization time; decreasing, *e.g.*, τ_0 to 0.8 fm/c (which is close to the overlap time of the 2 colliding nuclei at SPS energies) increases the QGP contribution at $q_T = 2$ GeV by ∼50%, which is less than 10% of the Drell-Yan contibution at all masses considered.

For the dilepton contribution from correlated decays of D and $\bar{D}$ mesons we use the experimental result from p-p collisions extrapolated to In-In, as provided by the NA60 collaboration [13]. As a note of caution, we remark that recent measurements at the Relativistic Heavy-Ion Collider (RHIC) report substantial modifications of heavy-quark spectra in Au-Au collisions, relative to p-p (as inferred from a suppression and elliptic flow of "non-photonic" single-electron spectra associated with semileptonic decays of open-charm (and -bottom) hadrons) [75, 76]. Such (possibly nonperturbative [77]) medium modifications of the charm momentum spectra presumably translate into a softening of the invariant-mass spectra of l^+l^- pairs as well. At the SPS, the shorter QGP lifetime is likely to lead to smaller effects, but an explicit measurement of the (delayed) charm decays has been presented recently [78].

IV. THERMAL FIREBALL EVOLUTION

Our description of the space-time evolution of central and semicentral A-A collisions is approximated by an expanding thermal fireball characterized by a time dependent cylindrical volume as [24],

$$V_{\mathrm{FB}}(t) = \pi \left(r_{\perp,0} + \frac{1}{2} a_\perp t^2 \right)^2 \left(z_0 + v_{z,0} t + \frac{1}{2} a_z t^2 \right) \, , \qquad (32)$$

where we neglect effects due to a finite ellipticity. The initial transverse radius $r_{\perp,0}$ is determined by the centrality of the collision (*e.g.*, $r_{\perp,0} = 5.15(4.6)$ fm for central (semicentral) In-In collisions). The initial longitudinal size, z_0, is equivalent to the formation time, τ_0, of the thermal medium, which we fix at the standard value of $\tau_0 = 1$ fm/c (translating into $z_0 \simeq \tau_0 \Delta y = 1.8$ fm, where $\Delta y = 1.8$ represents the rapidity width of a thermal fireball). For the longitudinal expansion we employ a moderate acceleration, $a_z = 0.045c^2$/fm, together with an initial velocity of $v_{z,0} = 0.6c$ (reminiscent to Ref. [24]), but the dilepton invariant-mass spectra are essentially unaffected if we use $(v_{z,0}, a_z) = (c, 0)$ as in Ref. [15]. The most important parameter is the transverse acceleration. More recent applications of the fireball model, both in the dilepton [15] and charm diffusion [77] context, have used larger values than in previous work [24, 38], in the range $a_\perp = 0.08 - 0.1c^2$/fm. Here, we employ $a_\perp = 0.085c^2$/fm as in Ref. [20].

The time evolution of the temperature is determined assuming entropy conservation. At a given collision energy, the hadro-chemistry of the fireball is characterized by thermal-model fits to the observed hadron ratios. In our default scenario we assume the chemical freezeout temperature to coincide with the critical temperature for QGP formation, at $T_{\mathrm{ch}} = T_c = 175$ MeV. For central and semicentral In(158A GeV)+In collisions we fix the entropy per (net) baryon at $s/\varrho^{\mathrm{net}}_B = 27$, which, using a hadronic resonance gas (HG) equation of state (EoS), translates into an associated baryon chemical potential of $\mu^{\mathrm{ch}}_B = 232$ MeV, well within the uncertainties of recent thermal model fits at SPS [21, 22] (all other chemical potentials being zero). The subsequent hadronic trajectory in the phase diagram is then constructed at fixed $s/\varrho^{\mathrm{net}}_B = 27$ (isentropic expansion) with the additional constraints of pion, kaon, η and antibaryon number conservation, requiring the build-up of corresponding chemical potentials. For a given number of nucleon participants (*i.e.*, collision centrality), the fireball entropy amounts to $S = 2630(1890)$ for central (semicentral) In-In collisions, translating into a charged particle multiplicity of $\mathrm{d}N_{\mathrm{ch}}/\mathrm{d}y \simeq 195(140) \simeq N_{\mathrm{part}}$ (for a chemical freezeout temperature of $T_{\mathrm{ch}} = 160$ MeV, as considered below, the multiplicities increase by less than 5%). Using the relation between the total entropy and volume, $S = s(t) \cdot V(t)$, the entropy density, $s(t)$, can be used to determine the time evolution of temperature and baryon density (along the hadronic trajectory) using the HG

EoS, and similarly for the QGP phase using a quasiparticle EoS. The volume partition in the HG-QGP mixed phase is calculated from the standard mixed-phase construction, where the fraction of matter in the hadronic phase is given by

$$f_{\rm HG}(t) = \frac{s_c^{\rm QGP} - s(t)}{s_c^{\rm QGP} - s_c^{\rm HG}} \ , \qquad (33)$$

where $s_c^{\rm HG,QGP}$ denote the critical entropy densities at T_c. With a formation time of $\tau_0 = 1$ fm/c, the evolution for central (semicentral) In-In starts in the QGP at $T_0 =$ 197(190) MeV, passes through a mixed phase at $T^{\rm ch} = T_c = 175$ MeV, and terminates at thermal freezeout at around $T_{\rm fo} \simeq$ 120-135 MeV.

The main uncertainties associated with the fireball evolution are the transverse acceleration as well as the overall lifetime (which is somewhat correlated to the longitudinal expansion). It turns out that the latter is rather sensitive to the absolute magnitude of the experimentally observed dilepton excess radiation, resulting in $\tau_{\rm fo} \simeq 6$ fm/c for central In-In collisions. The remaining uncertainty consists of the interplay between longitudinal and transverse expansion. As mentioned above, the variations considered in our previous works [15, 20], $a_\perp = 0.08$-$0.085\,c^2$/fm and $(v_z^0, a_z) = (c, 0)$-$(0.6c, 0.045\,c^2/{\rm fm})$, have negligible impact on the invariant mass spectra, while the longitudinal-acceleration scenario, which we will focus on here, allows for a slightly larger transverse expansion which appears to be favored by the rather hard q_T spectra. In principle, more accurate information on the final state of the expansion can be obtained once hadronic spectra for In-In are available (our pion spectra are actually in reasonable agreement with S-Au data, recall lower panel of Fig. 6). For central Pb-Pb collisions at SPS energies, the typical results for transverse surface velocity and thermal freezeout temperature are $(\beta_\perp^s/c, T_{\rm fo}[{\rm MeV}]) = (0.65 \pm 0.1, 120 \pm 10)$ [79–82], which is quite comparable to the values used here for In-In. We emphasize that all contributions to the dilepton spectrum (QGP, ρ, ω, ϕ, and four-pion) are tied to the *same* evolution, thus fixing their relative weights.

Finally, to illustrate the uncertainties associated with the underlying equation of state we will investigate three combinations of critical and chemical freezeout temperatures roughly covering the current theoretical and experimental ranges:

(A) Our default scenario, employed in most of our calculations thus far, consisting of identical T_c and $T_{\rm ch}$ at an "intermediate" value of 175 MeV; thermal freezeout is fixed at $(\mu_\pi^{\rm fo}, T_{\rm fo}) = (79, 120)$ MeV (semicentral In-In).

(B) A scenario with a relatively small and identical critical and chemical freezeout temperature at $(\mu_B^{\rm ch}, T_{\rm ch}) = (240, 160)$ MeV, compatible with recent thermal model fits in Refs. [21, 22]. For dilepton spectra the most important consequences of this scenario are a significantly extended QGP phase which will increase its thermal emission contribution and reduce the hadronic one, in particular at intermediate masses. In addition, due to smaller pion chemical potentials in the subsequent hadronic phase, the freezeout temperature (at fixed fireball lifetime) will be larger than with EoS-A, at $(\mu_\pi^{\rm fo}, T_{\rm fo}) = (37, 136)$ MeV.

(C) A scenario with a large critical temperature $T_c = 190$ MeV (as suggested by recent lattice QCD computations [23], which maximizes (minimizes) the space-time volume occupied by the hadronic (QGP) phase. Since chemical freezeout at such a temperature is questionable, we allow for a chemically equilibrated hadronic phase until chemical-freeze out sets in under the same conditions as in EOS-B, at $(\mu_B^{\rm ch}, T_{\rm ch}) = (240, 160)$ MeV.

V. COMPARISON TO DILEPTON SPECTRA AT SPS

We now turn to a systematic analysis of experimental dilepton spectra as measured at the SPS by the NA60 and CERES/NA45 collaborations in In-In and Pb-Au collisions, respectively. Based on the various ingredients developed in the previous sections, we first address the NA60 invariant-mass and transverse-momentum spectra, followed by a consistency check with earlier and updated CERES data.

A. Invariant Mass Spectra

Thermal $\mu^+\mu^-$ invariant-mass spectra for A-A collisions are computed by integrating the emission rate, Eq. (1), over the fireball evolution (as well as three-momentum),

$$\frac{{\rm d}N_{ll}}{{\rm d}M} = \frac{M}{\Delta y} \int_0^{t_{\rm fo}} {\rm d}t\, V_{\rm FB}(t) \int \frac{d^3q}{q_0}\, \frac{{\rm d}N_{ll}}{{\rm d}^4x\, {\rm d}^4q} z_P^n {\rm Acc}(M, q_T, y) \ , \qquad (34)$$

where Acc denotes the detector acceptance which has been carefully tuned to NA60 simulations [83]. The fugacity factor, $z_P^n = {\rm e}^{n\mu_P/T}$, arises due to chemical off-equilibrium in the hadronic phase for $T < T_{\rm ch}$; it depends on the thermal emission source under consideration, cf. Eq. (4): for the ρ, ω and four-pion contributions one has z_π^n with $n = 2, 3, 4$, respectively, while for the ϕ one has $z_K^2 \cdot \gamma_s^2$, where $\gamma_s \simeq 0.75$ accounts for strangeness undersaturation for medium-size nuclear collision systems at the SPS [84]. In addition, appropriate fugacities figure into the various in-medium selfenergy contributions.

Initial comparisons [13] of NA60 data to theoretical predictions [14] have focused on the contribution from

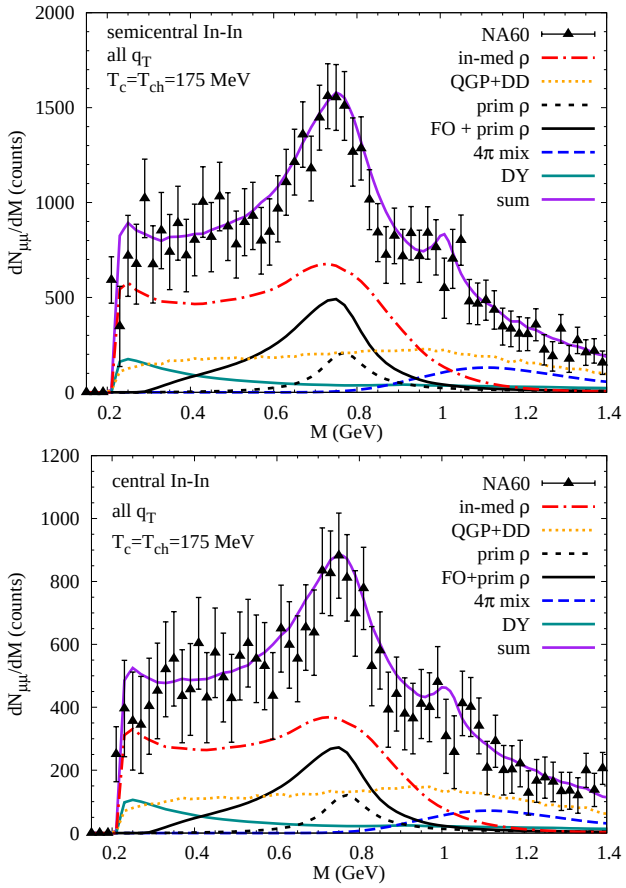

FIG. 7: (Color online) NA60 excess dimuon spectra [13] in semicentral (upper panel) and central (lower panel) In-In collisions at SPS compared to theoretical calculations using an in-medium e.m. spectral function. The individual contributions arise from in-medium ρ-mesons [24] (dash-dotted red line), 4π annihilation with chiral V-A mixing (dashed blue line), QGP plus correlated open charm decays (dotted orange line) and Drell-Yan annihilation (solid turquoise line); the upper dashed brown line is the sum of the above, while the solid purple line additionally includes in-medium ω and ϕ decays as well as freezeout plus primordial ρs (solid black line). In the semi-central data, the uncertainty due to the η cocktail subtraction is indicated by the open and filled data points (the former are based on an estimated η yield at high q_T while the latter represent an upper limit on the η by subtracting the dimuon spectrum to zero at threshold).

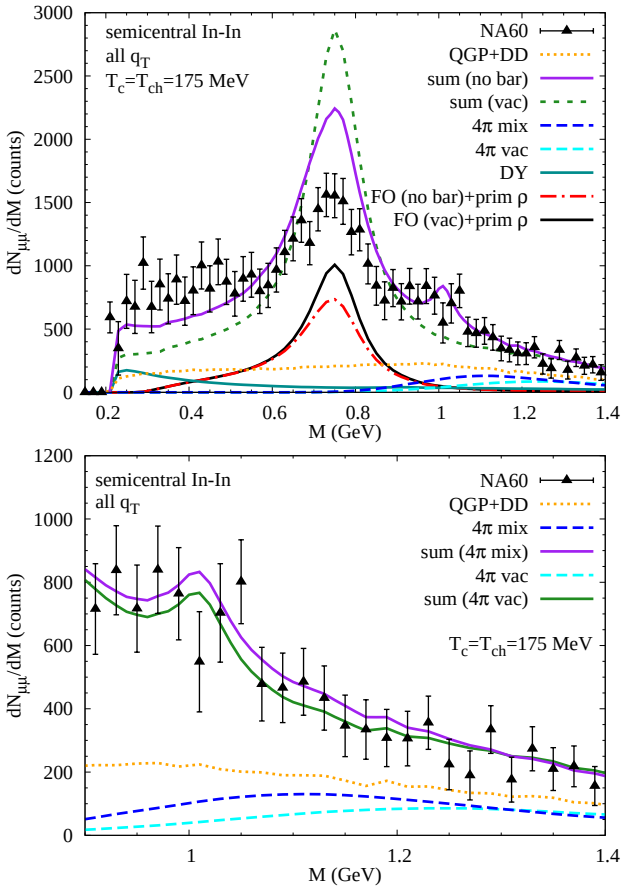

FIG. 8: (Color online) Upper panel: NA60 data [13] compared to thermal dimuon spectra using (i) in-medium ρ-, ω- and ϕ-mesons without baryon effects (+QGP+charm+in-medium four-pion; solid purple line), and (ii) free ρ (+QGP+charm+free four-pion; dashed green line). Lower panel: NA60 data [13] in the IMR compared to thermal dimuon spectra with different implementations of the four-pion contribution, using either its vacuum form (lower dashed line) or including chiral mixing (upper dashed line), and corresponding total spectra (lower and upper solid line, respectively).

the ρ meson which dominates in the LMR. The shape of the in-medium ρ-spectral function describes the experimental spectra well, but the absolute yields have been overestimated by $\sim 30\%$. This discrepancy has been resolved [15] by increasing the transverse fireball expansion ($a_\perp$), reducing the fireball lifetime to about 6-7 fm/c, cf. Sec. IV above. In addition, the larger transverse expansion leads to harder emission spectra in q_T, which will be helpful in understanding the q_T spectra, as discussed in the following sections.

Fig. 7 summarizes our results for the mass spectra in semicentral and central In(158 AGeV)-In collisions, computed for the EoS-A scenario ($T_c = T_{\rm ch} = 175$ MeV). The modifications relative to our previous work [15] are: (i) the freezeout ρ has been separated from the in-medium ρ contribution, (ii) primordial ρ and (iii) Drell-Yan contributions have been added. As a result of the separation (i), the thermal emission lifetime is now slightly smaller, 6.5(6.2) fm/c for central (semicentral) collisions. The inclusive mass spectra (and pertinent conclusions) are essentially identical to those in Ref. [15], *i.e.*, the predicted in-medium effects on ρ spectral function lead to good agreement with the data in the LMR, while the same fireball evolution also reproduces the observed excess in the IMR well. The largest source here is four-pion annihilation, together with smaller contributions from open-charm decays and QGP emission. In-medium ϕ decays are noticeable but not very significant relative to the un-

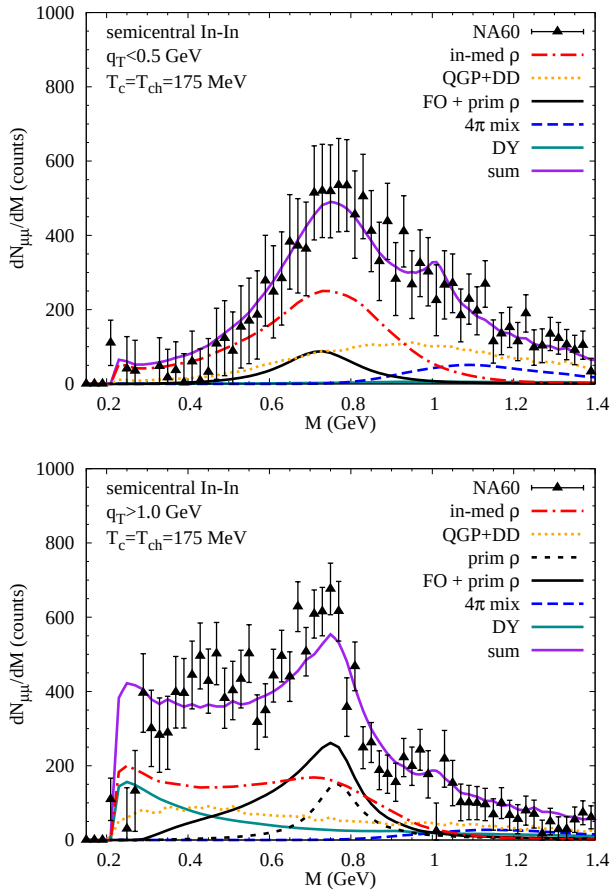

FIG. 9: (Color online) Dimuon invariant mass spectra in two different bins of transverse pair momentum, q_T [13]. Upper panel: $q_T \leq 0.5$ GeV; lower panel: $q_T \geq 1.0$ GeV.

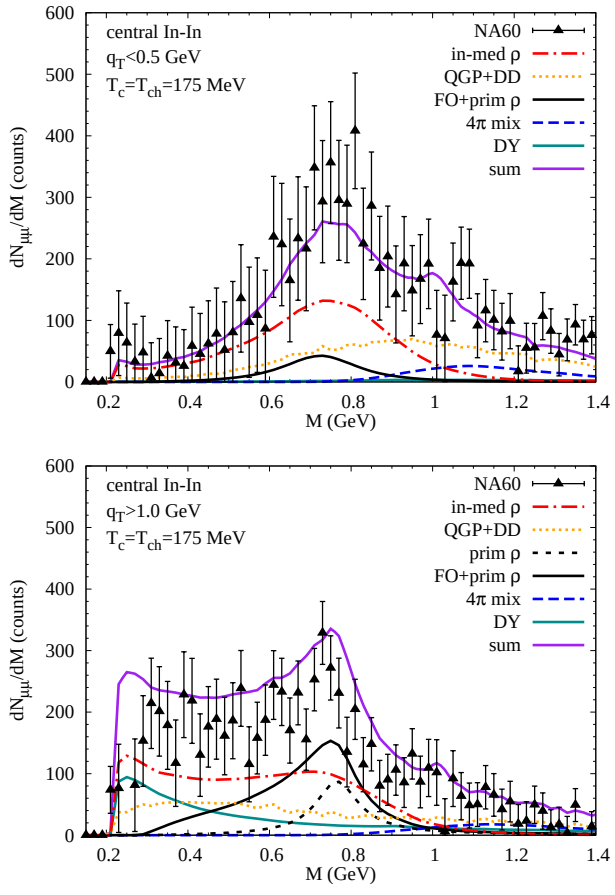

FIG. 10: (Color online) The same as Fig. 9 but for central collisions.

certainty in the data.

The sensitivity to the medium effects in the e.m. correlator is further illustrated in Fig. 8. The upper panel demonstrates that a free ρ spectral function is ruled out, but also one which only includes modifications due to a meson gas clearly does not reproduce the data, due to both a too narrow peak and a lack of enhancement below the free ρ mass, especially when approaching the dimuon threshold. In the lower panel one sees that the effect of chiral mixing on the 4π contribution amounts to up to a factor of $\sim$2 enhancement in the a_1 resonance region, but the effect on the total is rather moderate. Thus, no strong case on the chiral mixing can be made at present. The prevalence of the four-pion contribution in the IMR is reminiscent to the hydrodynamic calculations in Ref. [16] where hadronic rates calculated in the chiral reduction formalism have been employed. On the contrary, in the fireball calculations of Ref. [17] QGP emission dominates in the IMR. We elucidate on this discrepancy in Sec. V C below.

In Figs. 9 and 10 we compare our theoretical calculations to NA60 M-spectra binned into regions of low ($q_T < 0.5$ GeV) and high ($q_T > 1.0$ GeV) transverse pair momentum, for both semicentral and central collisions. Also in this representation the agreement is fair. There is possibly an indication of a slight over- (under-) estimate in the high-q_T bin for (semi-) central collisions. To further scrutinize this issue we now turn to q_T spectra, binned in invariant mass.

B. Transverse Momentum Spectra

In analogy to Eq. (34) for M spectra, q_T spectra are computed by integrating the dilepton rate, Eq. (1), over the space-time evolution of the fireball and a suitable interval in invariant mass, $[M_{\rm min}, M_{\rm max}]$. However, since the available experimental spectra have been corrected for the detector acceptance, the Monte-Carlo simulation of the acceptance function (with radial and angular dependencies due to directed (radial flow) and random (thermal) motion of the virtual photon) is now replaced by explicit integrations over the radial coordinate, r, of the fireball, the azimuthal angle, ϕ_q, of the virtual photon

momentum and its rapidity, y,

$$\frac{\mathrm{d}N_{ll}}{q_T \mathrm{d}q_T} = \int_0^{t_{\rm fo}} \mathrm{d}t \int_0^{R(t)} \mathrm{d}r \int_{M_{\rm min}}^{M_{\rm max}} \mathrm{d}M \int_0^{2\pi} \mathrm{d}\phi_q \int_{y_<}^{y_>} \mathrm{d}y \, 2\pi r \; z(t) \times M \; z_P^n \; \frac{\mathrm{d}N_{ll}}{\mathrm{d}^4x \mathrm{d}^4q} \; . \tag{35}$$

As before, $R(t)$ denotes the radius of the expanding fire-cylinder (corresponding to the first parenthesis in Eq. (32)), $z(t)$ its longitudinal length (second parenthesis in Eq. (32)). Note that the rate, Eq. (1), is calculated in the thermal rest frame while the integrations in Eq. (35) are in the laboratory frame. The relation between the four-momentum, q^μ, in the laboratory frame and the one in the local rest frame of the fluid cells, $\bar{q}^\mu$, is determined by a boost with the radial flow velocity, Eq. (23). Due to rotational invariance the thermal rate, Eq. (1), depends only on the magnitude of the three-momentum in the thermal rest frame and therefore one of the integrations over the spatial and momentum azimuthal angles in Eq. (35) becomes trivial yielding a factor of 2π. To gain qualitative insights into the behavior of dilepton q_T spectra from thermal sources, let us assume that the three-momentum dependence of the hadronic e.m. current correlator is weak (it would be absent in the absence of medium effects), so that for not too large invariant-mass intervals, the integrand in Eq. (35) can be considered constant except for the Bose distribution. For $M \gg T$, it is possible to approximate the qualitative behavior of the q_T spectra in analytic form [85, 86]. For a linear flow profile, Eq. (23), and in Boltzmann approximation one has

$$\frac{\mathrm{d}N_{ll}}{q_T \mathrm{d}q_T \mathrm{d}M \mathrm{d}t} = C \int_0^{R(t)} \mathrm{d}r \int_0^{2\pi} \mathrm{d}\phi \int_{-\infty}^{\infty} \mathrm{d}y \times r \exp\left(-\frac{q_0 - |\beta_\perp| q_T \cos\phi}{T\sqrt{1-\beta_\perp^2}}\right), \tag{36}$$

with C weakly q_T dependent. Substituting $q_0 = m_\perp \cosh y$ ($m_T = \sqrt{M^2+q_T^2}$) the integrals over y and ϕ are given by modified Bessel functions. For the y-integral we can use their asymptotic form for $m_T/T \geq M/T \gg 1$:

$$\frac{\mathrm{d}N_{ll}}{q_T \mathrm{d}q_T \mathrm{d}M \mathrm{d}t} = C \int_0^{R(t)} \mathrm{d}r \, r \sqrt{\frac{2\pi T\sqrt{1-\beta_\perp^2}}{m_T}} \times \exp\left(-\frac{m_T}{T\sqrt{1-\beta_\perp^2}}\right) I_0\left(\frac{|q_T||\beta_\perp|}{T\sqrt{1-\beta_\perp^2}}\right). \tag{37}$$

In the non-relativistic limit, $q_T \ll M$, we use the asymptotic form $I_0(x) \cong_{x\to 0} 1 + x^2/4 \simeq \exp(x^2/4)$ to obtain

$$\frac{\mathrm{d}N_{ll}}{q_T \mathrm{d}q_T \mathrm{d}M \mathrm{d}t} \underset{q_T \ll M}{\cong} C \int_0^{R(t)} \mathrm{d}r \, r \sqrt{\frac{2\pi T\sqrt{1-\beta_\perp^2}}{m_T}} \times \exp\left(-\frac{m_T}{T\sqrt{1-\beta_\perp^2}} + \frac{q_T^2\beta_\perp^2}{4T^2(1-\beta_\perp^2)}\right). \tag{38}$$

We have numerically verified that this expression can be further simplified by the following approximate treatment of the r integral: In the pre-factor of the exponential substitute $\beta_\perp$ by its average over r,

$$\langle \beta_\perp \rangle = \frac{2}{R^2} \int_0^R \mathrm{d}r r \beta_\perp^s \frac{r}{R} = \frac{2}{3}\beta_\perp^s \; ; \tag{39}$$

use the r average of the argument in the exponential, which, together with the non-relativistic approximation $q_T \cong_{q_T \ll M} \sqrt{2M(m_T - M)}$, results in

$$\frac{\mathrm{d}N_{ll}}{q_T \mathrm{d}q_T \mathrm{d}M \mathrm{d}t} \underset{q_T \ll M}{\cong} C \sqrt{2\pi T\sqrt{1-\langle\beta_\perp\rangle_r^2}} \times \exp\left(-\frac{M^2(\beta_\perp^s)}{2T^2}\right) \times \sqrt{\frac{1}{m_T}} \exp\left(-\frac{m_T}{T_{\rm eff}}\right) \tag{40}$$

where

$$T_{\rm eff} = \frac{T}{1-(M-T)(\beta_\perp^s)^2/(4T)} \underset{\beta_\perp^s \to 0}{\cong} T + \frac{M}{2}\left\langle \beta_\perp^2 \right\rangle_r , \tag{41}$$

and $\left\langle \beta_\perp^2 \right\rangle_r = (\beta_\perp^s)^2/2$. The form for $\beta_\perp^s \ll 1$ is the known "pocket formula" for the parametric dependence of the effective slopes of hadronic q_T spectra on the fireball temperature, the particle mass and the surface-flow velocity [86]. We recall that in the ultrarelativistic limit, $q_T \gg M$, the dependence of the effective temperature on the radial velocity is given by the Doppler blue-shift expression for a thermalized gas of massless particles,

$$T_{\rm eff}(\beta_\perp) = T\sqrt{\frac{1+\beta_\perp}{1-\beta_\perp}} \; , \tag{42}$$

which follows from the large-q_T limit of I_0 in Eq. (37) [86] which also provides an additional factor $1/\sqrt{q_T}$. For our r-dependent flow profile the effective temperature is given by the blue-shift value for an average value $\langle\beta_\perp\rangle_r = \xi\beta_\perp^s$ where $\xi \in (0,1)$ is not easily determined by simple approximations of the radial integral. Numerical studies show that in the case of a linear radial-flow profile, Eq. (23), and typical parameters in the region of the ρ peak ($M = 0.75$ GeV, $\beta_\perp^s \simeq 0.5$), $\xi \simeq 0.8$-0.85 leads to a good estimate for $T_{\rm eff}$ at high q_T.

It is important to note that for vector-meson decays after thermal freezeout, cf. Sec. III A), the q_T spectra are harder by an additional factor m_T/M, *i.e.*, applying the same approximations to Eq. (22) as used to derive Eq. (40), one obtains

$$\frac{\mathrm{d}N_{ll}^{(\mathrm{fo})}}{q_T \mathrm{d}q_T \mathrm{d}M} \underset{q_T \ll M}{\cong} C\sqrt{2\pi T\sqrt{1-\langle\beta_\perp\rangle_r^2}} \times \exp\left(-\frac{M^2(\beta_\perp^s)^2}{2T^2}\right) \times \frac{\sqrt{m_T}}{M}\exp\left(-\frac{m_T}{T_{\mathrm{eff}}}\right)\frac{1}{\Gamma_\rho^{(\mathrm{fo})}} \tag{43}$$

with T_{eff} again given by Eq. (41).

The additional factor m_T/M in (43) compared to (40) originates from the additional factor q^0/M in the Cooper-Frye (CF) formula (22) compared to the McLerran-Toimela (MT) emission formula (1), as discussed in detail in Sec. III A.

The above discussion of effective slopes in thermal emission spectra obviously does not apply to non-thermal dilepton sources, *i.e.*, decays of "primordial ρ mesons" (Sec. III B) and Drell-Yan annihilation (Sec III C). Both are characterized by a power-law behavior at high q_T, where their contribution becomes potentially important. Toward lower q_T, the primordial ρ contribution is much suppressed due to ρ absorption ("jet quenching"), while the Drell-Yan process is no longer well-defined. However, the Drell-Yan dileptons carry the hardest slope of all sources considered, which renders even a naive extrapolation of their spectra to low q_T very small (no more than a few percent for $q_T \leq 1$ GeV in all mass bins below $M = 1.4$ GeV). At $q_T \simeq 2$ GeV, in turn, the Drell-Yan contribution is quite appreciable.

Figs. 11 and 12 summarize our calculations for semicentral and central In-In collisions, respectively, in three different mass bins in comparison to the NA60 data [18]. Open-charm decays have been removed from the experimental spectra and are consequently not included in the theory curves either. The parameters of our fireball evolution are as described in Sec. IV within our default EoS-A scenario ($T_c = T_{\mathrm{ch}} = 175$ MeV). Since the overall normalization of the experimental spectra is not known at present, we have fixed it in each mass bin using the invariant mass spectra in the low-q_T bin ($0 \leq q_T \leq 0.5$ GeV). This easily translates into a 10-20% uncertainty in the absolute normalization. For the central collisions the agreement between theory and data is quite satisfactory in all mass bins. In the high-mass bin 1 GeV$\leq M \leq$1.4 GeV, lower panel in Fig. 12), this procedure appears to overestimate somewhat the q_T spectra at $q_T \geq 1$ GeV, which, however, seems not to be reflected in the corresponding q_T bin in the mass spectra (lower panel in Fig. 10). This could very well be due to the uncertainty in the underlying normalization procedure. Note again that the compared to Ref. [15] additionally implemented hard components (primordial ρ's and Drell-Yan) are insignificant at $q_T \leq 1$ GeV, *i.e.*, for the total

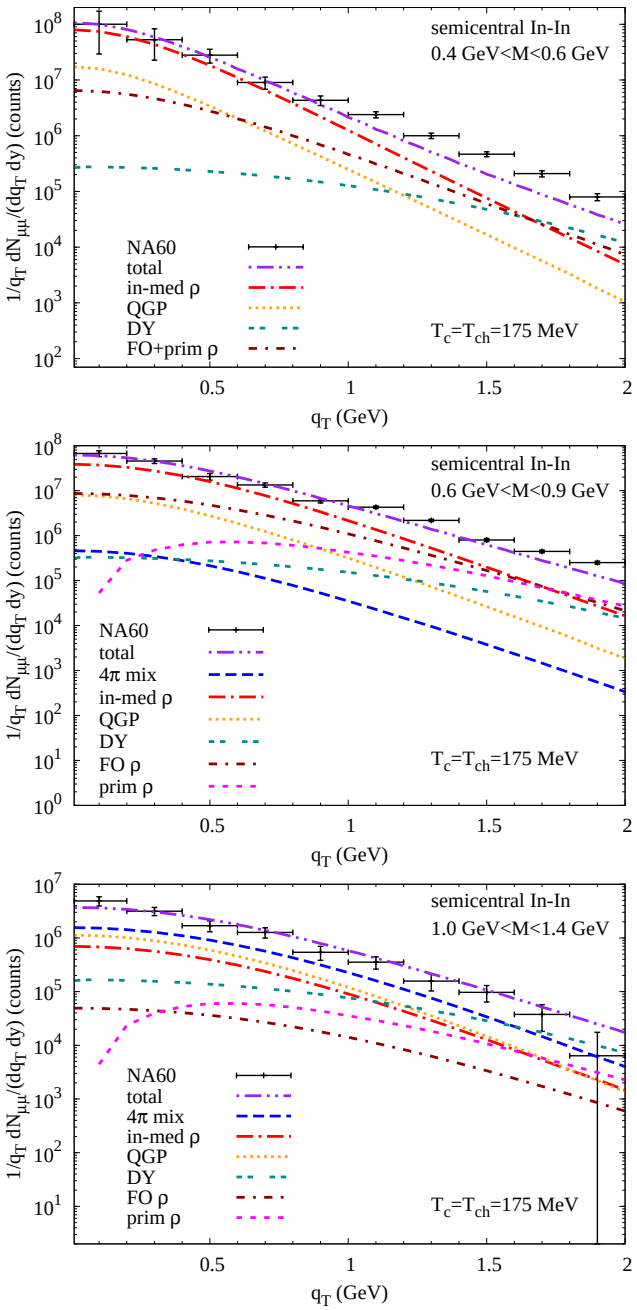

FIG. 11: (Color online) Dimuon transverse pair-momentum spectra in semicentral In(158 AGeV)-In collisions for three bins of invariant mass [18]. Upper panel: 0.4 GeV $\leq M \leq$ 0.6 GeV; middle panel: 0.6 GeV $\leq M \leq$ 0.9 GeV; lower panel: 1.0 GeV $\leq M \leq$ 1.4 GeV.

yield and the understanding of the spectral shape of the inclusive M-spectra. On the other hand, at higher q_T, these contributions are essential (even dominant) for a proper description of the spectra. In fact, in semicentral collisions, the experimental transverse momentum spectra in the two mass bins below (0.4 GeV$\leq q_T \leq$ 0.6 GeV) and around (0.6 GeV$\leq q_T \leq$ 0.9 GeV) the free ρ-meson mass turn out to be underestimated (and too soft) for

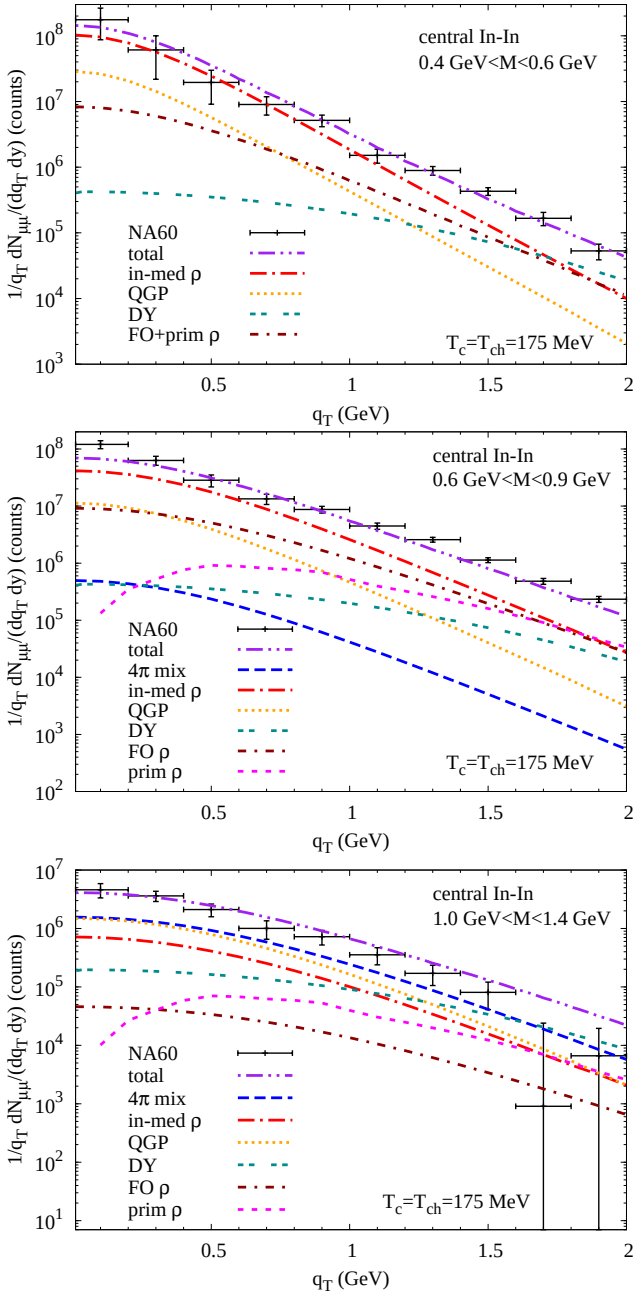

FIG. 12: (Color online) Same as Fig. 11, but for central In(158 AGeV)-In.

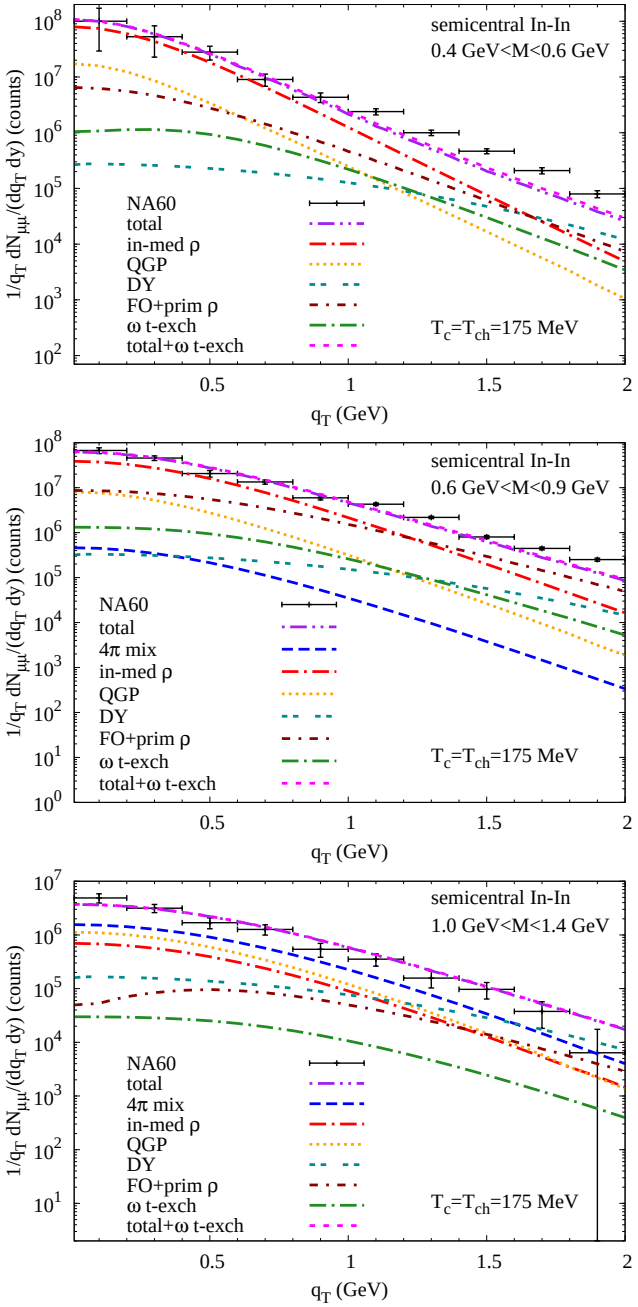

FIG. 13: (Color online) Same as Fig. 11, but additionally including (factor 2 augmented) contributions from ω t-channel exchange in $\pi\rho \to \pi\mu\mu$.

$q_T \gtrsim 1$ GeV. Especially in the low-mass bin, the discrepancy again appears to be larger than one could anticipate from the mass spectrum in the 0.4-0.6 GeV regime in the $q_T \geq 1$ GeV bin (lower panel in Fig. 9). The fact remains, however, that the theoretical q_T spectra in the low and intermediate mass bin are somewhat too soft. Even though the final transverse flow velocity of the fireball model is about 7% smaller for semicentral relative to central In-In collisions, this difference would not be able to account for the discrepancy (it amounts to a change in slope by about 10 MeV for the freeze-out ρ, and even less for thermal radiation). The nuclear suppression factor, $R_{AA}(q_T)$, in Fig. 6 (solid line) suggests that there might be room for a 30% increase of the primordial plus freezeout ρ contribution (possibly more if one could compare to the R_{AA} of ρ mesons; due to their larger mass a more pronounced flow effect could enhance their R_{AA}). Whether this would suffice in the low-mass bin, is questionable.

Another possibility consists of meson t-channel exchange in elastic scattering of ρ mesons off pions in

the heat bath (with subsequent conversion into a lepton pair). These processes have been calculated previously for real photon production [11] (which are given by the same diagrams except that the final-state photon is on-shell), where ω exchange has been found to be the most important process at high q_T; however, contributions from other exchange processes (*e.g.*, π and a_1 exchange in $\pi\rho \to \pi\gamma$, or reactions involving strange mesons [11]) are also appreciable. To roughly account for the latter, we augment the rates computed in Sec. II D by a factor of two (in addition, we recall that $\pi\rho$ initial states in the hadronic fireball emission carry a pion fugacity factor to the third power, z_π^3). The convolution of these rates over the fireball evolution leads to a contribution to dilepton-q_T spectra as shown by the lower dash-dotted line in each of the panels in Fig. 13; it indeed provides the hardest spectrum among all thermal sources (QGP, in-medium vector mesons and four-pion annihilation), in line with the rates displayed in Fig. 5. Consequently, the relative importance of the t-channel processes grows with q_T but remains rather moderate even at $q_T \simeq 2$ GeV, up to 15% and 5% of the total theoretical yield in the M = 0.4-0.6 GeV and 0.6-0.9 GeV mass bins, respectively (negligible for $M > 1$ GeV). Note that the slopes of the t-channel emission spectra resemble the data quite well, but our present estimate of their strength is insufficient to resolve the discrepancies at high q_T. However, their impact on the slope of the total spectra is not insignificant, as we will see in Sec. V D below.

C. Hadro-Chemical Freezeout and Critical Temperature

In all our calculations of thermal dilepton spectra thus far, the medium evolution was based on the notion that the critical (T_c) and chemical freezeout ($T_{\rm ch}$) temperature coincide, at $T_c = T_{\rm ch} = 175$ MeV. More recent theoretical (lattice QCD) and phenomenological (thermal model fits to hadron ratios) studies, however, allow for the possibilities that T_c could be significantly larger (190-200 MeV) and $T_{\rm ch}$ significantly smaller (150-160 MeV). While a smaller $T_c \simeq 160$ MeV is still viable, a larger $T_{\rm ch}$ appears unlikely since in a high-density hadronic phase number-changing reactions affecting the chemistry are to be expected (in addition, thermal model fits start to become unstable at temperatures above ∼180 MeV due to uncertainties in the high-lying, high degeneracy hadron resonance spectrum). Therefore, in this section we study the sensitivity of the invariant-mass and q_T spectra to the hadro-chemistry of the fireball, keeping its geometry and flow parameterization as well as the total lifetime the same as before (including all normalizations, where applicable). As quoted in Sec IV, in addition to our standard equation of state (EoS-A: $T_c = T_{\rm ch} = 175$ MeV), we investigate two alternative scenarios: EoS-B with $T_c = T_{\rm ch} = 160$ MeV and EoS-C with $T_c = 190$ MeV, $T_{\rm ch} = 160$ MeV. In general, a lower chemical freezeout temperature (where all meson chemical potentials are by definition zero) entails a larger volume at chemical freezeout, and thus also smaller baryon chemical potentials (*i.e.*, smaller baryon densities), as well as smaller meson chemical potentials in the subsequent evolution. This furthermore implies that, to obtain roughly the same overall dilepton yield, thermal freezeout occurs at a *larger* temperature (and smaller $\mu_{\pi,K}$), which, in principle, leads to (somewhat) harder q_T spectra, both at thermal freezeout and for thermal emission throughout the hadronic evolution. In the remainder of this Section, we focus on semicentral collisions.

We start our investigation within the "EoS-B" scenario, *i.e.*, $T_c = T_{\rm ch} = 160$ MeV. The resulting M- and q_T-spectra are compiled in Figs. 14 and 15, respectively. The smaller T_c implies a longer duration of both the QGP and mixed phase (the latent heat for EoS-B is larger than for EoS-A since entropy density for the QGP EoS drops slower with T than for the HG EoS), while the duration of the hadronic phase is accordingly reduced. As noted above, the thermal-freezeout temperature has increased to $T_{\rm fo} = 136$ MeV (compared to $T_{\rm fo} = 120$ MeV for EoS-A). As an immediate consequence, QGP radiation is significantly enhanced, while the hadronic yield is slightly reduced (both for in-medium ρ in the LMR and four-pion in the IMR). The overall quality in the description of the invariant-mass spectra is quite comparable to the EoS-A scenario. The somewhat harder spectra implied by the larger hadronic temperatures for EoS-B (most notably for the freezeout ρ) lead to a slight increase of the dilepton yield in the ρ mass region in the $q_T \geq 1$ GeV momentum bin (compare lower panels in Figs. 9 and 14). However, in the low- (0.4 GeV$\leq M \leq$ 0.6 GeV) and intermediate-mass (0.6 GeV$\leq M \leq$ 0.9 GeV) bins of the q_T spectra, the improvement at high q_T is rather marginal, while in the higher mass (1.0 GeV$\leq M \leq$ 1.4 GeV) there is essentially no change compared to the EoS-A calculation (recall Fig. 11), despite the fact that the QGP contribution is now larger than the four-pion one.

Turning to the EoS-C scenario (summarized in Figs. 16 and 17), the large value of $T_c = 190$ MeV leads to a QGP and mixed phase which is shorter than for EoS-A, but there is now a "high-density" (chemically equilibrated) hadronic phase down to $T_{\rm ch} = 160$ MeV, followed by a subsequent chemical off-equilibrium evolution which is identical to EoS-B. Obviously, the QGP emission yield is the smallest of all three scenarios, while the hadronic yield (both in-medium ρ's and four-pion annihilation) is the largest, possibly implying a slight overestimate in the ρ-mass region of the inclusive mass spectra (13% larger than for EoS-A, which could be readjusted by a slightly reduced lifetime). The high-density hadronic phase helps in the q_T spectra in the low- and intermediate-mass bin, for which, at high q_T, the discrepancy is the smallest for the three scenarios. In the highest mass bin, even the rather large ratio of four-pion annihilation over QGP emission does not upset the agreement with the q_T spectra, indicating that a large part of the four-pion emission

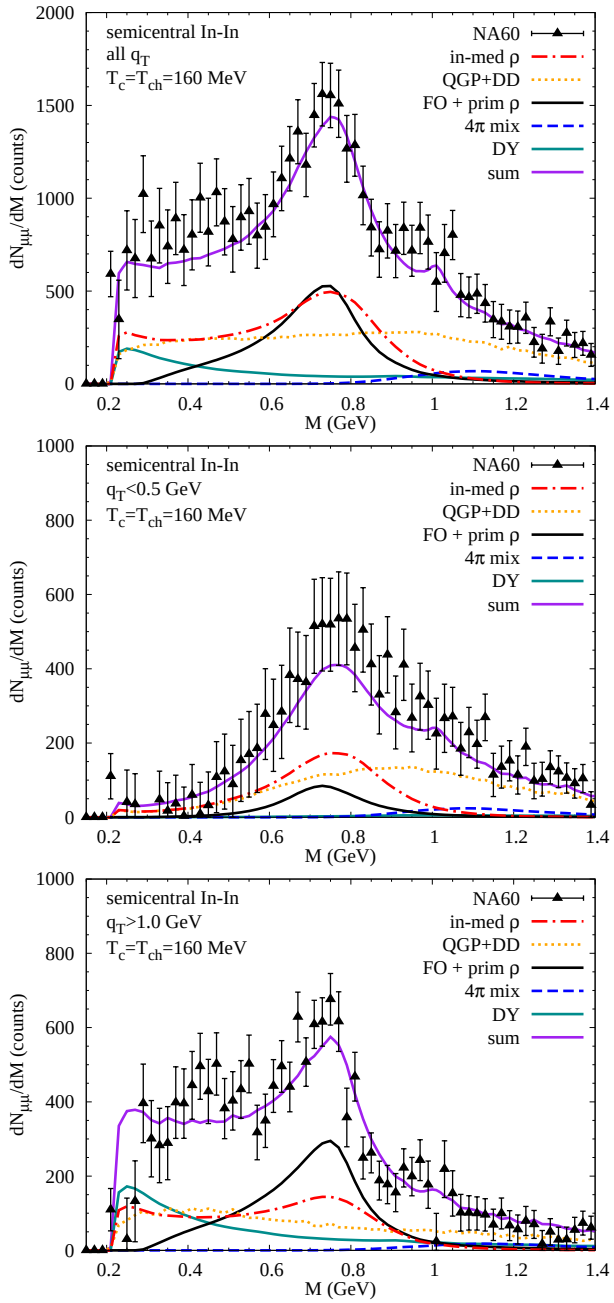

FIG. 14: (Color online) The same as Fig. 9, but for a fireball with a critical temperature T_c = 160 MeV and a chemical-freezeout temperature $T_{\rm ch}$ = 160 MeV (EoS-B).

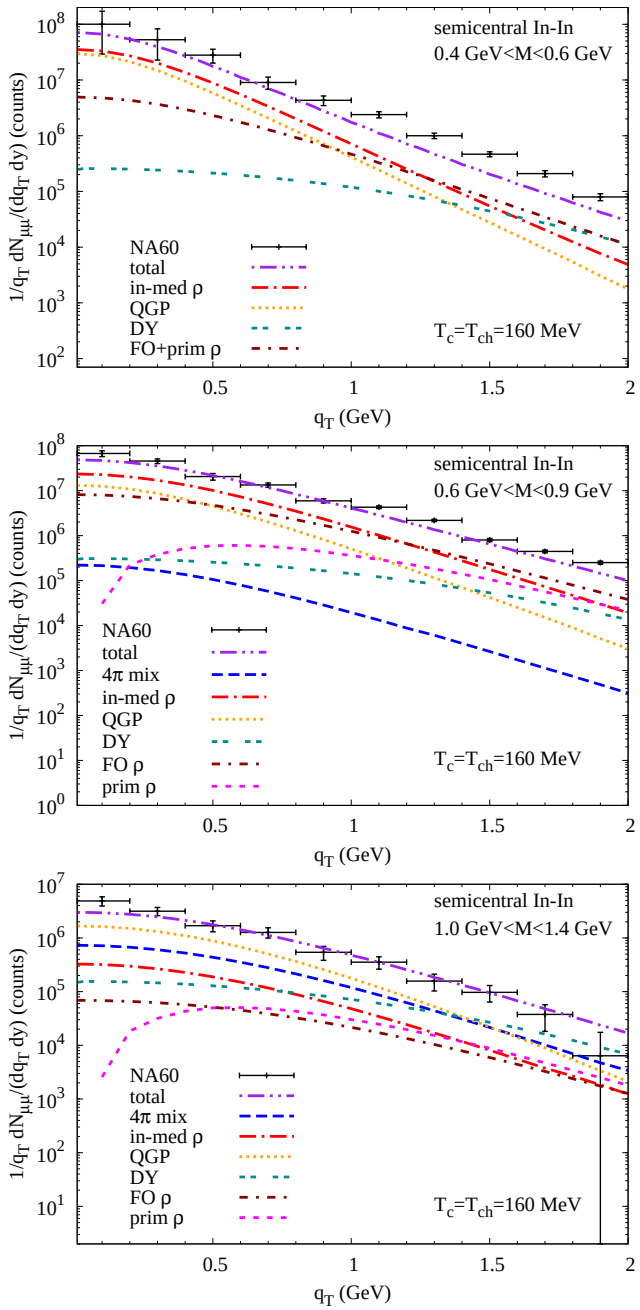

FIG. 15: (Color online) The same as Fig. 11, but for a fireball with a critical temperature T_c = 160 MeV and a chemical-freezeout temperature $T_{\rm ch}$ = 160 MeV (EoS-B).

emanates from the high-density hadronic phase.

Since the question of four-pion vs. QGP emission in the IMR has drawn considerable attention in the recent literature [87], we take a closer look at their interplay in our three scenarios in Fig. 18. The plot illustrates again that with EoS-B ($T_c = T_{\rm ch} = 160$ MeV) the QGP contribution exceeds the in-medium four-pion annihilation over the entire IMR considered (note that the tails of the ρ spectral function are not included). The opposite trend applies to our default EoS-A scenario, and even more so for EoS-C. Especially the large difference between EoS-B and EoS-C clearly demonstrates that the major portion of the four-pion emission emanates from the high-density hadronic phase (EoS-B and EoS-C have an identical hadronic evolution below $T_{\rm ch} = 160$ MeV); a similar argument applies to EoS-A, *i.e.*, four-pion emission does not primarily arise in the late stages (with large flow) despite an enhancement through large pion-fugacity factors. The basic reason for this can be understood by inspecting the temperature-mass differential emission

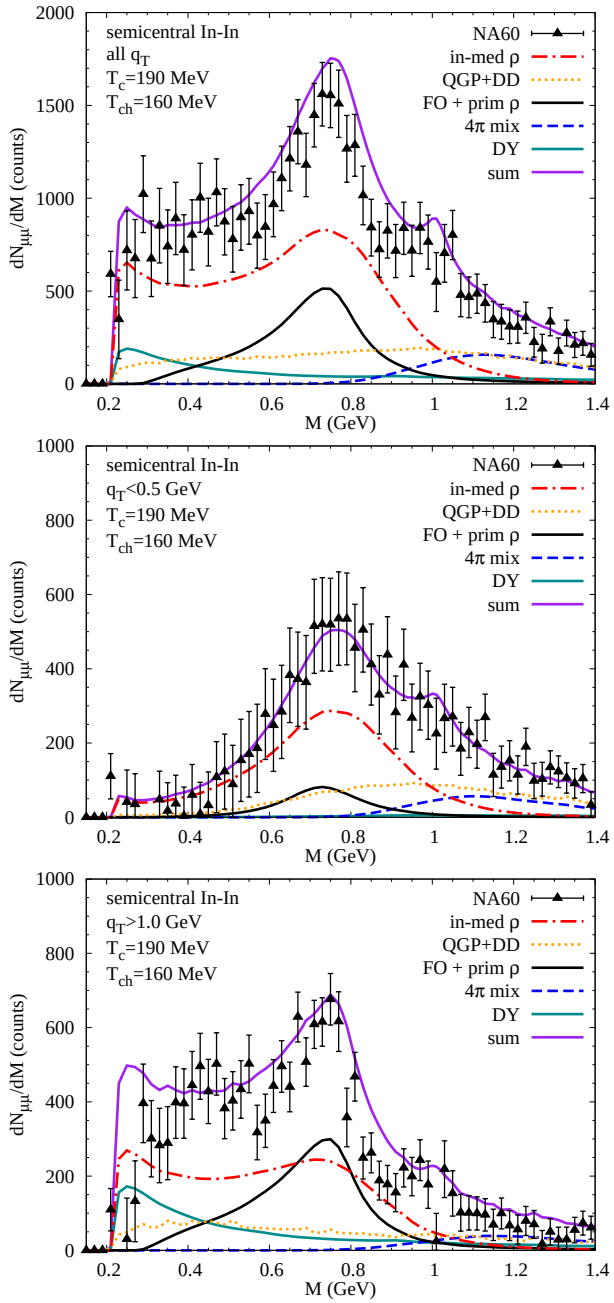

FIG. 16: (Color online) The same as Fig. 9, but for a fireball with a critical temperature $T_c = 190$ MeV and a chemical-freezeout temperature $T_{\rm ch} = 160$ MeV (EoS-C).

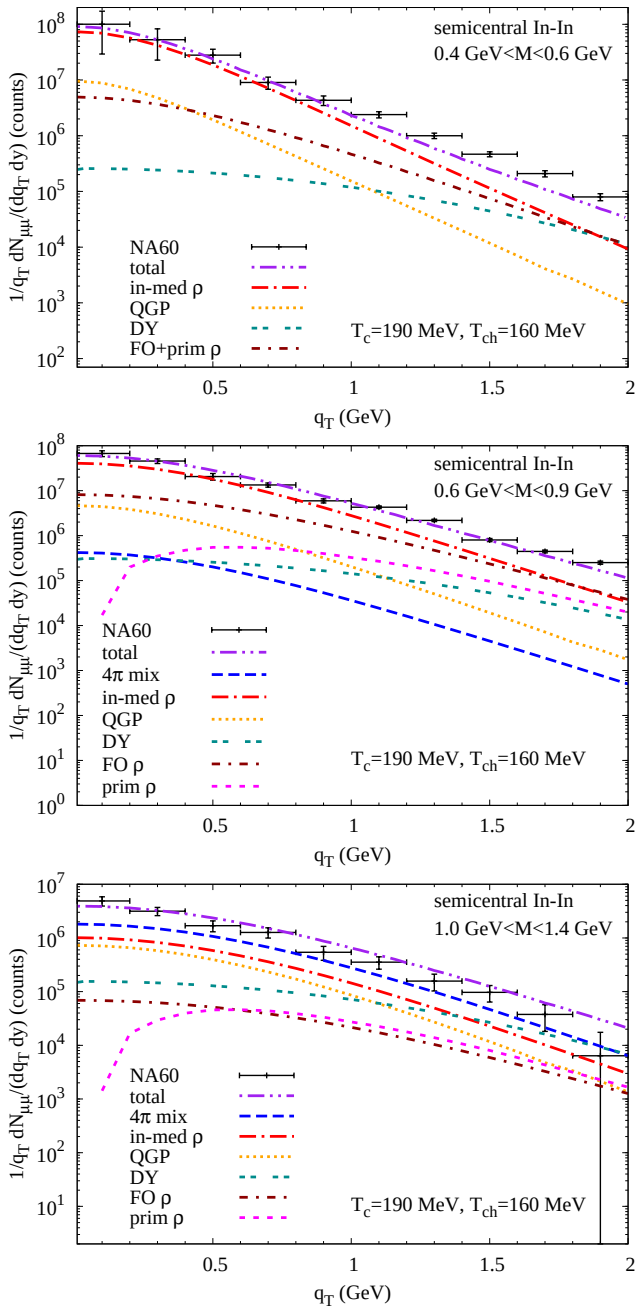

FIG. 17: (Color online) The same as Fig. 11, but for a fireball with a critical temperature $T_c = 190$ MeV and a chemical-freezeout temperature $T_{\rm ch} = 160$ MeV (EoS-C).

yield which is roughly given by [14]

$$\frac{{\rm d}N_{ll}}{{\rm d}M{\rm d}T} \propto {\rm Im}\,\Pi_{\rm em}(M,T)\ {\rm e}^{-M/T}\ T^{-5.5}\ , \qquad (44)$$

characterized by the standard thermal exponential factor and a power in temperature resulting from the three-momentum integral over the Boltzmann factor and, most importantly, the volume expansion. Assuming a weak temperature dependence of the e.m. spectral function (medium effects bias the emission toward higher T), a differentiation over T identifies the temperature of maximum emission as $T_{\rm max} \simeq M/5.5$. In the IMR of interest here, this means a $T_{\rm max}$ right around T_c (note that, at T_c, the hadronic phase has an extra "advantage" of a roughly twice larger volume compared to the QGP due to the latent heat), consistent with our fireball emission pattern.

We conclude this section by noting that "reasonable" variations in hadro-chemical freezeout and critical temperature have a very moderate impact on the invariant-

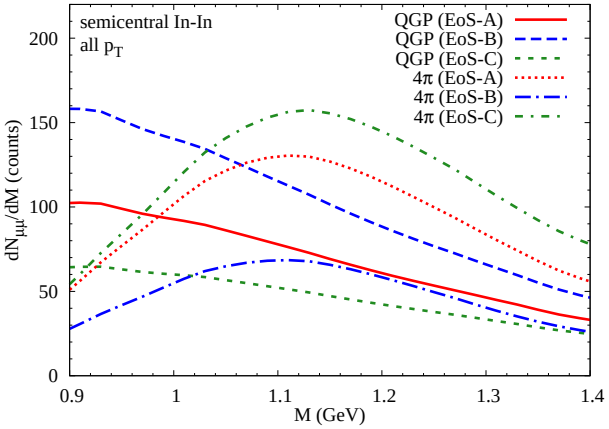

FIG. 18: (Color online) Comparison of the QGP and four-pion contributions to the dilepton yield in the intermediate mass region for the three equations of state, as discussed in the text. The 2-pion part, which is significant up to $M \simeq 1.1$ GeV, is not shown.

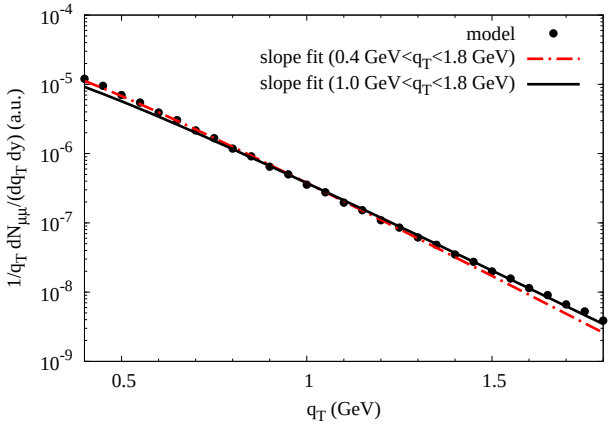

FIG. 19: (Color online) Dependence of the effective-slope fits, Eq. (45), to our theoretical q_T spectra without the Drell-Yan contribution (dots) on the fit range in q_T (as indicated in the legends) for the mass bin 0.3 GeV $\leq M \leq$ 0.4 GeV.

mass spectra as seen by NA60. On the one hand, this implies little sensitivity to the concrete values of T_c and $T_{\rm ch}$. On the other hand, it means that our results are very robust with respect to uncertainties in these quantities. The main reason for this robustness is the "quark-hadron duality" of the underlying (medium-modified) emission rates from the hadronic and QGP phase in the relevant temperature regime, $T = 160$-190 MeV, in both LMR (ρ melting) and IMR (including chiral mixing). As such, it provides additional support to the medium modifications in the employed rates. In the IMR, this "duality" does not allow for a (maybe even academic) distinction between a high-density hadronic or partonic source. Partitions with either component dominant are viable in both mass and transverse momentum spectra. Concerning the high-q_T region of the lower two mass bins, our calculations indicate a slight preference for EOS-B and EOS-C, due to their smaller $T_{\rm ch}$, implying larger temperatures in the hadronic evolution.

D. Slope analysis

To complete our analysis of the q_T spectra we perform in this section a quantitative analysis of effective slope parameters following the procedure adopted by the NA60 collaboration for the experimental data [18, 87, 88]. The q_T spectra have been divided into several invariant-mass bins, in each of which the data have been fitted to the function

$$\frac{1}{q_T}\frac{{\rm d}N}{{\rm d}q_T} = \frac{1}{m_T}\frac{{\rm d}N}{{\rm d}m_T} = C\exp\left(-\frac{m_T}{T_{\rm eff}}\right)\,, \qquad (45)$$

where the fit range is typically taken as 0.4 GeV $< q_T <$ 1.8 GeV, but the extracted slopes are rather insensitive to variations as long as the lower limit is above 0.4 GeV. In addition, the experimental q_T spectra exhibit little dependence on centrality (except for peripheral collisions), and therefore the slope analysis has been performed for inclusive q_T spectra with ${\rm d}N_{\rm ch}/{\rm d}y > 30$. In our theoretical analyses we focus on semicentral collisions.

We have tried to follow the same procedure (see also Ref. [89], but as illustrated by the dash-dotted line in Fig. 19, a fit to our theoretical spectra (represented by the dots) in the above range (0.4 GeV $< q_T <$ 1.8 GeV) slightly underestimates the effective slopes toward higher q_T, especially in the lower mass bins. Part of the problem is the bias of the fit toward low q_T where the yield is the largest and thus dominates the total χ^2. To better reproduce the theoretical spectral shape with the above function we have therefore chosen to (i) restrict the fit range to 1 GeV $< q_T <$ 1.8 GeV, and (ii) minimize the χ^2 for the logarithm of the spectra. The resulting fit (solid line in Fig. 19) indeed agrees better with the theoretical spectra. This effect becomes more pronounced when the Drell-Yan component is included (which, in fact, might indicate that our extrapolation overestimates the DY yield at low mass).

Based on the slightly revised procedure, our slope analysis is carried out for the total sum of all calculated q_T spectra components in twelve $\Delta M = 0.1$ GeV mass bins in the range 0.2 GeV $< M <$ 1.4 GeV (corresponding to the experimental ones) for semicentral In-In; by default, the Drell-Yan and meson t-channel contributions are not included, but studied in separate fits by adding them to the totals. As in the experimental analysis, correlated open-charm decays are removed altogether. Our systematic study addresses variations in the EoS as well as the possibility of another ∼15% increase in the transverse acceleration of the fireball expansion, *i.e.*, $a_\perp = 0.1c^2/{\rm fm}$ (which is, in fact, the value we have used in our calculations for heavy-flavor observables at RHIC [77], as extracted from the hydrodynamic model of Ref. [95]). Specifically, we evaluate the following scenarios, as sum-

marized in the six panels of Fig. 20:

(a) the default fireball expansion with EoS-A ($T_c = T_{\rm ch} = 175$ MeV), characterized by a thermal freeze-out with temperature and radial flow surface velocity of $(T_{\rm fo}, \beta^s_{\perp,{\rm fo}}) = (120\ {\rm MeV}, 0.57c)$;

(b) the default fireball expansion with EoS-B ($T_c = T_{\rm ch} = 160$ MeV) and $(T_{\rm fo}, \beta^s_{\perp,{\rm fo}}) = (136\ {\rm MeV}, 0.57c)$;

(c) the default fireball expansion with EoS-C ($T_c = 190$ MeV, $T_{\rm ch} = 160$ MeV) and $(T_{\rm fo}, \beta^s_{\perp,{\rm fo}}) = (136\ {\rm MeV}, 0.57c)$;

($\rm b^+$) the same as in (b), but with a transverse fireball acceleration $a_\perp = 0.1\,c^2/{\rm fm}$ yielding $(T_{\rm fo}, \beta^s_{\perp,{\rm fo}}) = (135\ {\rm MeV}, 0.65c)$;

($\rm c^+$) the same as in (c), but with a transverse fireball acceleration $a_\perp = 0.1\,c^2/{\rm fm}$ yielding $(T_{\rm fo}, \beta^s_{\perp,{\rm fo}}) = (135\ {\rm MeV}, 0.65c)$;

($\rm c_1^{++}$) the same as in ($\rm c^+$), but additionally including the contribution from meson-t-channel exchange with in-medium ρ propagator (cf. Sec. II D);

($\rm c_2^{++}$) the same as in ($\rm c_1^{++}$), but using the vacuum ρ propagator in the meson-t-channel exchange contribution.

The upper two panels of Fig. 20 compare the impact of the three different EoS using our baseline acceleration of $a_\perp = 0.085c^2/{\rm fm}$. The default scenario EoS-A (a) falls short of the empirical slopes by a significant margin of up to 50-60 MeV in the LMR, while reaching the lower end of the data in the IMR. The higher hadronic temperatures of scenarios EoS-B (b) and EoS-C (c) improve the situation by about 15-20 MeV in the LMR, approximately reflecting the increase in the hadronic fireball temperatures (e.g., $T_{\rm fo} = 136$ MeV compared to $T_{\rm fo} = 120$ MeV at thermal freezeout). Scenario EoS-B (b) additionally improves around the ρ peak due to a larger weight of the relatively hard components from decays of freezeout and primordial ρ, since the overall thermal hadronic emission is smaller than for EoS-A and EoS-C (compare Fig. 15 to Figs. 7 and 16). However, for both EoS-B and EoS-C the slopes in the LMR are still below the data, even though the shape is not too bad.

In an attempt to improve on the slopes, we investigate a further increase of the transverse acceleration to values representative for RHIC energies [77, 95], from $0.085\ c^2/{\rm fm}$ to $0.1\ c^2/{\rm fm}$ for EoS-B and EoS-C (scenarios ($\rm b^+$) and ($\rm c^+$), shown in the middle panels of Fig. 20). While this increases the effective slopes at all emission stages, it is more efficient for the later hadronic sources (in accordance with the blue-shift pocket formulae given in Sec. V B). Consequently, the LMR exhibits further improvement, and, importantly, the consistency with the data in the IMR is not spoiled due to the fact that the main contributions there arise from earlier stages with higher temperatures and less flow (dominated either by the contributions from the QGP phase for EoS-B or four-pion annihilation in the high-density hadronic phase for EoS-C, cf. Fig. 18). At this point, EoS-B provides somewhat better agreement and one might be tempted to take this as evidence for a prevalently partonic emission source, as suggested in Refs. [87, 88]. However, remaining uncertainties preclude an unambiguous interpretation, as we will now show.

In the two bottom panels of Fig. 20 we focus on the EoS-C scenario with $a_\perp = 0.1c^2/{\rm fm}$. The left panel illustrates the sensitivity of the slopes to the additional inclusion of t-channel meson exchange processes. As discussed in the previous section, their spectra alone carry a slope very similar to the data; not surprisingly, their inclusion increases the slopes in the LMR with no impact on the IMR slopes. When implementing the t-channel meson exchanges with the vacuum ρ propagator, the effect on the slopes is somewhat larger compared to using the in-medium D_ρ, especially in the free ρ mass region. A single $\pi\rho$ scattering with unmodified ρ mesons would most closely represent interactions of ρ mesons in a kinetic regime (rescattering without thermalization), and thus provide a missing link between the two extremes of thermal radiation and primordial ρ's surviving jet quenching (no reinteraction) in our baseline calculations (note that there is no contribution from "quenched" ρ's). The overall level of agreement with the data is now very similar to EoS-B. Also recall that $T_c = 190$ MeV maximizes the ratio of hadronic to QGP emission; for $T_c = 175$ MeV four-pion emission still outshines the QGP in the IMR, while the slope parameters are closer to the EoS-B scenario. The effect of the Drell-Yan contribution on the slopes is shown in the bottom-right panel of Fig. 20. In the IMR the change in slope is consistent with the experimental results (full vs. open squares), while in the lowest mass bins the uncertainties in the extrapolation of the DY are large. We emphasize again that more stringent constraints can be enforced once an accurate knowledge of the absolute normalization in the experimental mass and momentum spectra becomes available.

There are uncertainties in the experimental extraction of the slope parameters beyond the statistical error bars shown in the figures. In Ref. [88] a systematic error of $\sim$7 MeV is estimated due to the subtraction of background and decay (cocktail) sources. For the LMR, it has been estimated that the subtraction of a potential Drell-Yan contribution could lower the effective slopes by 5-10 MeV. One should also be aware of that the applicability of hydrodynamic (or thermal fireball) descriptions is limited in transverse momentum, typically to $p_T \leq 2$ GeV for pion spectra at the SPS (consistent with where the spectra reach the collision-scaling regime in Fig. 6), and to significantly smaller p_T for elliptic flow. Fireball models might compensate for this to some extent by implementing a larger acceleration, which may be (part of) the reason that the dilepton slopes prefer

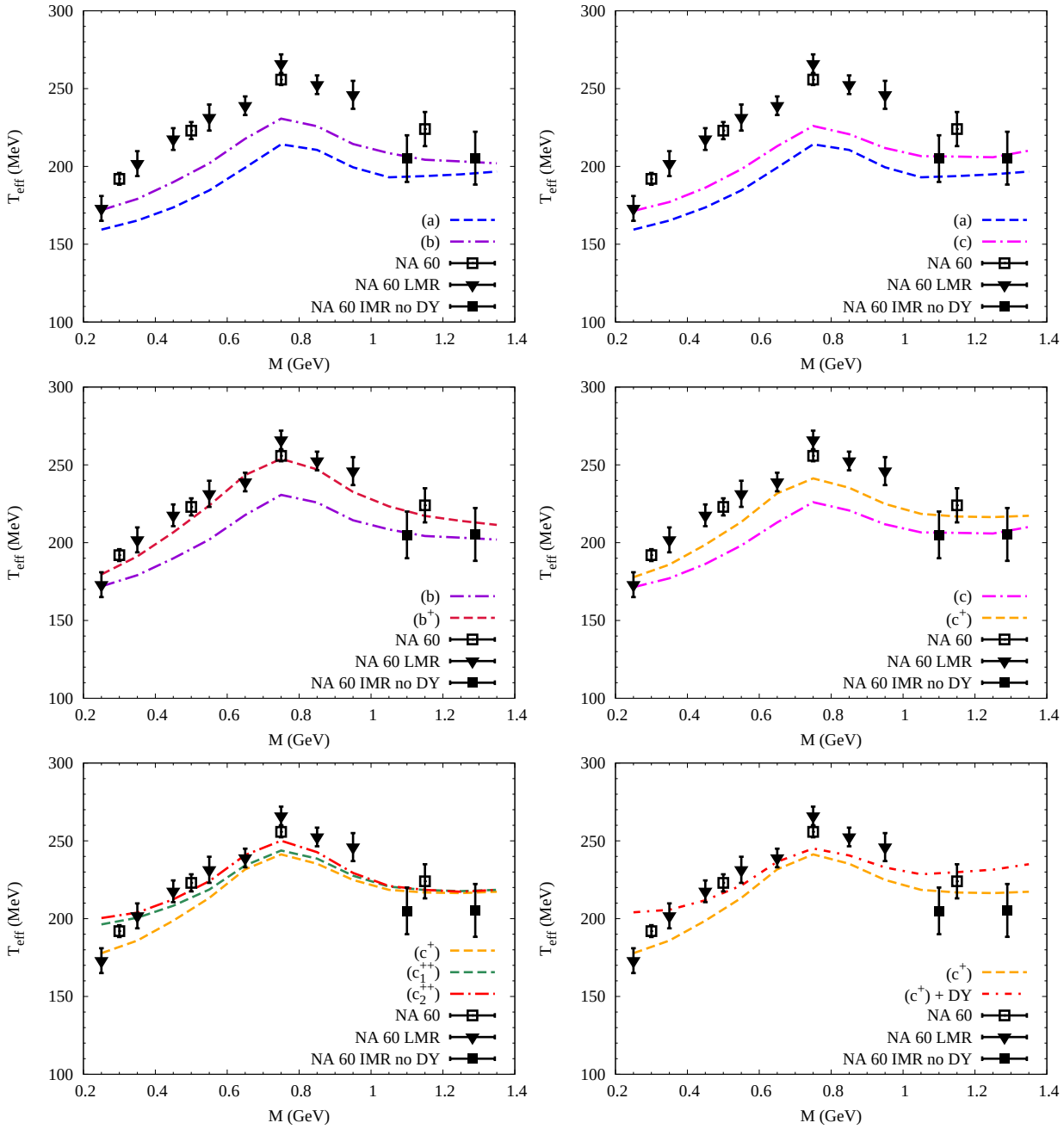

FIG. 20: (Color online) Effective slope parameters fitted to the theoretical q_T spectra using Eq. (45) for the following scenarios (by default, DY and t-channel meson exchange reactions are not included): top left: EoS-A (dashed line) vs. EoS-B (dash-dotted line), both with $a_\perp = 0.085c^2$/fm; top right: EoS-A (dashed line) vs. EoS-C (dash-dotted line), both with $a_\perp = 0.085c^2$/fm; middle left: EoS-B with either $a_\perp = 0.085c^2$/fm (dash-dotted line) or $a_\perp = 0.1c^2$/fm (dashed line); middle right: EoS-C with either $a_\perp = 0.085c^2$/fm (dash-dotted line) or $a_\perp = 0.1c^2$/fm (dashed line); bottom left: EOS-C with $a_\perp = 0.1c^2$/fm (lower dashed line), additionally including meson t-channel contributions with free (dash-dotted line) or in-medium (middle dashed line) ρ propagator; bottom right: EOS-C with $a_\perp = 0.1c^2$/fm (dashed line), additionally including Drell-Yan annihilation (dash-dotted line).

$a_\perp = 0.1c^2$/fm. To further scrutinize the q_T spectra, it would be very illuminating to reiterate earlier implementations of the dilepton rates from hadronic many-body theory into hydrodynamic [50] (with a more realistic hadro-chemsitry) or transport [49] simulations. In this context, a measurement of dilepton elliptic flow could provide further insights in the detailed emission history of the medium at SPS energies [90].

E. Update of Comparison to CERES/NA45 Data

After the refinements in our theoretical approach for SPS dilepton spectra in the context of the NA60 data, we revisit in this section the consequences for the comparison with CERES/NA45 in semicentral and central Pb-Au collisions, which showed good agreement in our earlier works [24, 36, 68]. In the following, we constrain ourselves to the above default scenario for the fireball evolution with a transverse acceleration of $a_\perp = 0.085\,c^2/\mathrm{fm}$. As in the In-In case, the increased expansion rate entails shorter fireball lifetimes; we choose the latter as to obtain the same thermal freezeout temperature for central ($T_{\rm fo} \simeq 106$ MeV) and semicentral ($T_{\rm fo} \simeq 112$ MeV) Pb-Au collisions as in our previous work [9, 24], implying a reduction by 2 fm/c for both centralities (13.5 $\to$ 11.5 fm/c and 12 $\to$ 10 fm/c, respectively). Also, since for the larger system sizes (*i.e.*, lifetimes) the freezeout- and cocktail-ρ contributions [4] are significantly suppressed relative to thermal radiation, and since we are not interested in (high-) q_t spectra here, we adopt the (old) simplified treatment for the freezeout ρ by running the fireball an additional duration of 1 fm/c [24]. The larger lifetimes relative to In-In collisions furthermore imply that the nonrelativistic formula for the surface expansion velocity, $v_\perp^s = a_\perp t$, approaches values uncomfortably close to c in the late stages of the collision. To implement a relativistically covariant acceleration in a simple way, we model the acceleration of the fireball in analogy to the relativistic motion for a charged particle in a homogeneous electric field. The radial surface velocity and fireball radius then take the form

$$\beta_\perp^s = \frac{a_\perp t/c}{\sqrt{1+a_\perp^2 t^2/c^2}}, \qquad r = r_0 + \frac{c^2}{a_\perp}\left(\sqrt{1+a_\perp^2 t^2/c^2} - 1\right) , \tag{46}$$

which tames the acceleration at late times and matches the non-relativistic case for early times.

In the upper panel of Fig. 21 the updated calculations for dielectron spectra in semicentral Pb-Au collisions are compared to our previous results (using the same hadrochemistry and ρ spectral function), including experimental acceptance cuts as defined by CERES/NA45. For masses $M \gtrsim 0.6$ GeV, the ρ spectral function yield is reduced by 15-20%, directly reflecting the reduction in the lifetime of the hadronic phase in the fireball. At lower masses, however, the difference is smaller and eventually disappears for $M \lesssim 0.35$ GeV. The reason for this is the interplay of the single-electron cuts and the increase in transverse flow, where the latter gives larger momentum to both electrons which in turn have a larger probability to make it into the acceptance. For the QGP contribution, the difference is smaller (less than 10%) and weakly dependent on mass, since the increased transverse flow plays little role in the early phases (we recall that, for the canonical choice of the formation time, $\tau_0 = 1$ fm/c, the initial temperature for 30% central Pb-Au amounts to $T_0 = 203$ MeV, and 210 MeV for 7% central). The addition of in-medium ω and ϕ decays affects the total yield mostly around the respective free masses, more significantly in the ϕ region. The in-medium four-pion contribution becomes relevant for masses $M \gtrsim 1$ GeV, with a relative strength compared to the other sources that closely resembles the In-In case. The Drell-Yan contribution does not show up on the scale of Fig. 21 (and has been restricted to masses above ~1 GeV). Correlated charm decays are not accounted for. The lower panel of

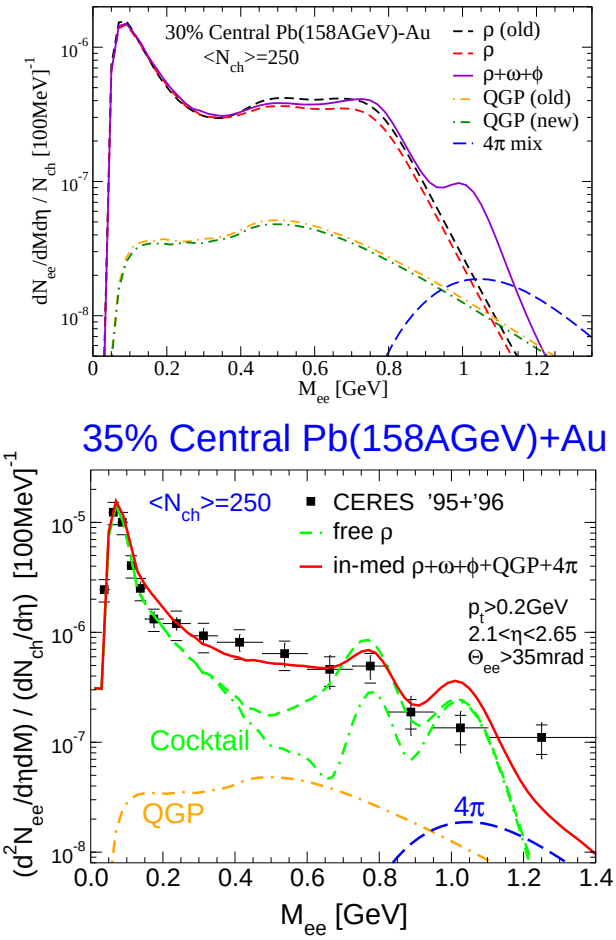

FIG. 21: (Color online) Upper panel: comparison of thermal dilepton spectra in semicentral Pb-Au collisions (including experimental acceptance) for ρ (short-dashed lines) and QGP emission (dash-dotted lines) using our previous (labeled "old") and updated fireball evolution. The solid line is the sum of in-medium ρ, ω and ϕ contributions, while the long-dashed line results from four-pion annihilation including chiral mixing as described in Sec. II C. The Drell-Yan contribution is below the displayed range; correlated charm decays are neglected. Lower panel: The solid line is the total in-medium thermal emission + hadronic cocktail (dash-dotted line, adopted from the experimental evaluation [4]), compared to combined 1995/1996 CERES/NA45 data [4]. The short-dashed line is the sum of thermal emission with a vacuum ρ spectral function and the cocktail.

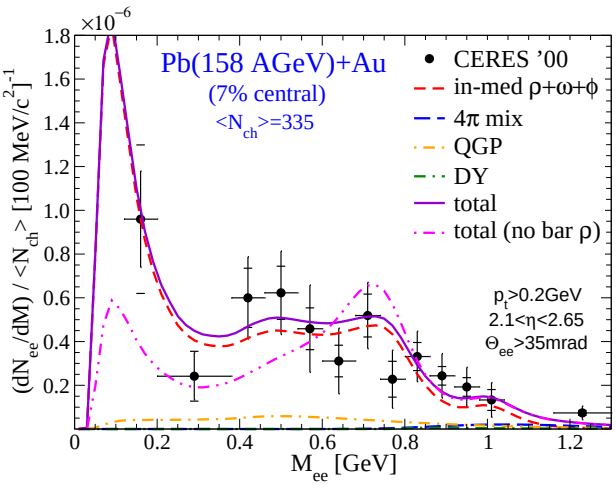

FIG. 22: (Color online) Comparison of theoretical calculations of dilepton excess spectra in central Pb-Au collision, compared to CERES/NA45 data [25]; for the line labeled "total (no bar ρ)" the full in-medium ρ spectral function has been replaced by the one which only includes medium effects in a meson gas.

Fig. 21 summarizes the comparison of the theoretical calculations with the combined 1996/1996 CERES/NA45 data [4], including the hadron decay cocktail. The level of agreement is very similar to the one with our earlier results [24, 68].

Finally, we turn to the most recent CERES data for central Pb(158 AGeV)-Au collisions [25], which are shown in Fig. 22 in a form similar to the NA60 data in the previous sections, *i.e.*, on a linear scale and with the cocktail subtracted. Again, our calculations employing the updated fireball describe these data fairly well. Variations of $\pm 20\%$ in the fireball lifetime (affecting the total dilepton yields at the same level with little change in the spectral shape), would still lead to reasonable agreement. The importance of baryon-induced medium modifications at SPS energies is reiterated by the dash-double-dotted curve where only meson-gas effects are included in the ρ spectral function; this scenario does not properly reproduce the experimental spectra. When comparing to the NA60 dimuon mass spectra, the four-pion and QGP contributions in the IMR appear smaller relative to the signal in the mass region below the free ρ mass. This is essentially due to the experimental acceptance, which for CERES/NA45 is significantly larger in the low-mass region than for NA60, especially for low-momentum lepton pairs.

A particularly striking feature of the theoretical predictions is the large enhancement below the two-pion threshold, which is closely connected with the approach to (and constraints from) the photon point. The very-low-mass excess is rather sensitive to the baryon-induced medium effects as well, as illustrated by the curve where the latter are switched off. Experimentally, this regime is only accessible with dielectrons (and after subtraction of the π^0 Dalitz decay), and the first hint from data is consistent with the theoretical yield. Clearly, it would be very worthwhile to further explore this region.

VI. SUMMARY AND CONCLUSIONS

In the present paper, we have conducted a quantitative study of dilepton spectra in semi-/central heavy-ion collisions at full SPS energy ($\sqrt{s} = 17.3$ GeV). We have supplemented our earlier calculations of thermal radiation (which reproduce available mass spectra) with sources of non-thermal origin (expected to become relevant at high transverse momentum and for small systems), and we have scrutinized the results with respect to hadrochemical and flow properties of the underlying thermal fireball expansion.

The key quantity to describe thermal dilepton rates is the (imaginary part of the) electromagnetic current correlator. In hadronic matter, we have evaluated its medium modifications in terms of many-body spectral functions for the light vector mesons at low mass, and chiral vector-axialvector mixing for the continuum part at intermediate mass. Partonic emission above T_c has been approximated by perturbative quark-antiquark annihilation. An appealing feature of this description is a smooth merging of the hadronic rates with the partonic ones at temperatures around the expected phase transition, $T_c = 160$-190 MeV. As a new ingredient we have computed thermal dilepton rates induced by t-channel meson exchange in $\pi\rho \to \pi l^+ l^-$ reactions, which we found to become relevant at momenta above $\sim$1.5 GeV. We have augmented our approach by non-thermal sources, *i.e.*, Drell-Yan annihilation, as well as decays of ρ mesons from primordial production (subject to jet quenching) and from decoupling at thermal freezeout. We have emphasized that these ρ decays carry an extra kinematic Lorentz-γ factor relative to thermal radiation, resulting in harder dilepton-q_T spectra.

All sources have been implemented into a space-time evolution for A-A collisions at SPS, for which we employed an isentropic fireball model with QGP, mixed and hadron-gas phases and updated expansion parameters to better match the absolute dilepton yields measured by NA60. Hadrochemical freezeout and subsequent evolution are constructed in line with measured hadron multiplicities. The calculated dimuon invariant-mass spectra agree well with NA60 data in central and semicentral In-In collisions, including q_T bins below 0.5 GeV and above 1.0 GeV, thus confirming our earlier results for thermal emission and validating the predicted in-medium vector spectral functions (dominated, but not exhausted, by the ρ). When comparing to q_T spectra, the new sources contribute to provide good agreement for central collisions, while discrepancies persist with semicentral data at $q_T > 1$ GeV for masses around and below the free ρ mass. In particular, effective slope parameters for $q_T \geq 1$ GeV amount to $T_{\rm eff} \simeq 160$-210 MeV, $\sim$25% short of the em-

pirically extracted values in the LMR.

We have investigated the sensitivity of our results to variations in the critical and chemical-freezeout temperature of the fireball. The spectral shape of the invariant-mass spectra turned out to be insensitive for the range $T_c = 160 - 190$ MeV. The reason is the "duality" of the thermal emission rates around T_c, rendering the "melting" of the ρ meson a robust signal. A low value of $T_c = 160$ MeV entails that QGP radiation dominates over hadronic emission in the IMR. A low value of $T_{\rm ch} = 160$ MeV implies smaller pion chemical potentials (and thus higher temperatures) in the hadronic evolution, increasing the effective slope parameters by about 15-20 MeV, still ∼30 MeV short of the data in the LMR.

In an attempt to resolve this discrepancy, we have implemented a ∼15% increase in the transverse fireball acceleration as previously employed for central Au-Au collisions at RHIC energy. This elevates the slope to ∼250 MeV around the free ρ mass (and properly reproduces the increase below), while still being consistent with the (upper) experimental value of 205 ± 20 MeV in the IMR where the blue shift effect is less pronounced due to the prevalently early emission. In particular, we have demonstrated that, within the current theoretical and experimental uncertainties, *both* scenarios for a predominant emission source in the IMR – hadronic (four-pion) or partonic – are viable. In either case, the radiation mostly emanates from matter at temperatures around $T_c \simeq 160 - 190$ MeV. An unambiguous distinction between a partonic and hadronic source in the IMR therefore appears difficult at SPS energies. The larger transverse flow developed in the partonic stage at RHIC energies could facilitate this task [91], although additional complications arise due to the much larger open-charm contribution and its in-medium modifications.

Finally we have checked that our refined assessment of dilepton sources, together with the improvements in the fireball expansion, preserves our previously found agreement with the CERES/NA45 dielectron spectra in Pb-Au collisions. The larger system size leads to an appreciable increase in thermal radiation, thus reducing the uncertainties associated with the modeling of the break-up stage. In addition, dielectrons allow access to the mass region below the two-pion threshold, where the medium effects on the ρ-spectral function, augmented by the thermal Bose factor (and photon propagator), predict a large thermal dilepton signal. First data in this region support this signal, and further corroborate the importance of baryonic interactions for the in-medium ρ spectral function.

Future efforts should be pursued along several directions: first and foremost, the theoretically calculated vector spectral functions must be extended to their chiral partners (most notably the axialvector (a_1) channel as the partner of the ρ), to establish direct connections to chiral symmetry restoration. The evaluation of in-medium Weinberg sum rules [92], in connection with constraints from lattice QCD, will play an important role in this enterprise [93, 94]. Second, from the phenomenological side, the implementation of emission rates into both hydrodynamic and transport simulations should be reiterated, to compute q_T spectra and check whether the rather large acceleration of the fireball model can be justified for the In-In system at SPS. The study of dilepton elliptic flow [90] could shed further light on the time profile of the radiation. At RHIC energies, partonic collectivity increases significantly; an unexpectedly large dilepton excess in the LMR recently observed by PHENIX needs to be understood [96]. Work in several of these directions is in progress.

Acknowledgments

We are grateful to S. Damjanovic and H. J. Specht for discussion and information on the NA60 acceptance, and to A. Marin for providing us with the new CERES data. This work was supported in part by a U.S. National Science Foundation CAREER award under grant no. PHY-0449489.

[1] R. Rapp and J. Wambach, Adv. Nucl. Phys. **25**, 1 (2000).
[2] J. Alam, S. Sarkar, P. Roy, T. Hatsuda, and B. Sinha, Annals Phys. **286**, 159 (2001).
[3] C. Gale and K. L. Haglin (2003), hep-ph/0306098.
[4] G. Agakichiev et al. (CERES Collaboration), Eur. Phys. J. C **41**, 475 (2005).
[5] D. Adamova et al. (CERES/NA45 Collaborations), Phys. Rev. Lett. **91**, 042301 (2003).
[6] A. L. S. Angelis et al. (HELIOS-3 Collaboration), Eur. Phys. J. C **13**, 433 (2000).
[7] M. C. Abreu et al. (NA38/NA50 Collaborations), Nucl. Phys. **A661**, 538 (1999).
[8] M. C. Abreu et al. (NA38 Collaboration), Eur. Phys. J. C **14**, 443 (2000).
[9] R. Rapp and E. V. Shuryak, Phys. Lett. B **473**, 13 (2000).
[10] M. M. Aggarwal et al. (WA98 Collaboration), Phys. Rev. Lett. **85**, 3595 (2000).
[11] S. Turbide, R. Rapp, and C. Gale, Phys. Rev. C **69**, 014903 (2004).
[12] R. Rapp (2002), nucl-th/0204003.
[13] R. Arnaldi et al. (NA60 Collaboration), Phys. Rev. Lett. **96**, 162302 (2006).
[14] R. Rapp, J. Phys. G **31**, S217 (2005).
[15] H. van Hees and R. Rapp, Phys. Rev. Lett. **97**, 102301 (2006).
[16] K. Dusling, D. Teaney, and I. Zahed, Phys. Rev. C **75**, 024908 (2007).
[17] J. Ruppert, C. Gale, T. Renk, P. Lichard, and J. I. Ka-

pusta (2007), arXiv:0706.1934 [hep-ph].
[18] S. Damjanovic et al. (NA60 Collaboration), Nucl. Phys. A **783**, 327 (2007).
[19] R. Rapp, H. van Hees, and T. Strong, Braz. J. Phys. **37**, 779 (2007).
[20] H. van Hees and R. Rapp, J. Phys. G **34**, S1051 (2007).
[21] A. Andronic, P. Braun-Munzinger, and J. Stachel, Nucl. Phys. A **772**, 167 (2006).
[22] F. Becattini, J. Manninen, and M. Gazdzicki, Phys. Rev. C **73**, 044905 (2006).
[23] F. Karsch, J. Phys. G **34**, S627 (2007).
[24] R. Rapp and J. Wambach, Eur. Phys. J. A **6**, 415 (1999).
[25] D. Adamova et al. (CERES Collaboration) (2006), nucl-ex/0611022.
[26] L. D. McLerran and T. Toimela, Phys. Rev. D **31**, 545 (1985).
[27] G.-Q. Li and C. Gale, Phys. Rev. C **58**, 2914 (1998).
[28] M. Harada and K. Yamawaki, Phys. Rept. **381**, 1 (2003).
[29] R. Barate et al. (ALEPH Collaboration), Eur. Phys. J. C **4**, 409 (1998).
[30] K. Ackerstaff et al. (OPAL Collaboration), Eur. Phys. J. C **7**, 571 (1999).
[31] S. Weinberg, Phys. Rev. Lett. **18**, 507 (1967).
[32] T. Das, V. S. Mathur, and S. Okubo, Phys. Rev. Lett. **19**, 859 (1967).
[33] M. Urban, M. Buballa, R. Rapp, and J. Wambach, Nucl. Phys. A **641**, 433 (1998).
[34] N. M. Kroll, T. D. Lee, and B. Zumino, Phys. Rev. **157**, 1376 (1967).
[35] J. J. Sakurai, *Currents and Mesons* (University of Chicago Press, Chicago, 1969).
[36] R. Rapp, G. Chanfray, and J. Wambach, Nucl. Phys. A **617**, 472 (1997).
[37] R. Rapp, M. Urban, M. Buballa, and J. Wambach, Phys. Lett. B **417**, 1 (1998).
[38] R. Rapp, Phys. Rev. C **63**, 054907 (2001).
[39] A. Schenk, Nucl. Phys. B **363**, 97 (1991).
[40] E. V. Shuryak, Nucl. Phys. A **533**, 761 (1991).
[41] R. Rapp and J. Wambach, Phys. Lett. B **351**, 50 (1995).
[42] H. van Hees and J. Knoll, Nucl. Phys. A **683**, 369 (2000).
[43] A. Gomez Nicola, F. J. Llanes-Estrada, and J. R. Pelaez, Phys. Lett. B **606**, 351 (2005).
[44] B. Friman (1998), nucl-th/9801053.
[45] R. Rapp and C. Gale, Phys. Rev. C **60**, 024903 (1999).
[46] S. Leupold, W. Peters, and U. Mosel, Nucl. Phys. A **628**, 311 (1998).
[47] V. L. Eletsky, M. Belkacem, P. J. Ellis, and J. I. Kapusta, Phys. Rev. C **64**, 035202 (2001).
[48] F. Riek and J. Knoll, Nucl. Phys. A **740**, 287 (2004).
[49] W. Cassing, E. L. Bratkovskaya, R. Rapp, and J. Wambach, Phys. Rev. C **57**, 916 (1998).
[50] P. Huovinen and M. Prakash, Phys. Lett. B **450**, 15 (1999).
[51] K. Reygers (PHENIX Collaboration), AIP Conf. Proc. **870**, 736 (2006), nucl-ex/0608043.
[52] W. M. Yao et al. (Particle Data Group), J. Phys. G **33**, 1 (2006).
[53] M. Wachs, Ph.D. thesis, Technische Universiät Darmstadt (2000), URL `http://elib.tu-darmstadt.de/diss/000050/`.
[54] D. Cabrera and R. Rapp (2007), work in progress.
[55] M. F. M. Lutz, G. Wolf, and B. Friman, Nucl. Phys. A **706**, 431 (2002).
[56] D. Trnka et al. (CBELSA/TAPS Collaboration), Phys. Rev. Lett. **94**, 192303 (2005).
[57] M. Kaskulov, E. Hernandez, and E. Oset, Eur. Phys. J. A **31**, 245 (2007).
[58] K. Haglin, Nucl. Phys. A **584**, 719 (1995).
[59] A. T. Martell and P. J. Ellis, Phys. Rev. C **69**, 065206 (2004).
[60] L. Alvarez-Ruso and V. Koch, Phys. Rev. C **65**, 054901 (2002).
[61] D. Cabrera, L. Roca, E. Oset, H. Toki, and M. J. Vicente Vacas, Nucl. Phys. A **733**, 130 (2004).
[62] T. Ishikawa et al., Phys. Lett. B **608**, 215 (2005).
[63] M. Dey, V.L. Eletsky, and B.L. Ioffe, Phys. Lett. B **252**, 620 (1990).
[64] J. V. Steele, H. Yamagishi, and I. Zahed, Phys. Rev. D **56**, 5605 (1997).
[65] M. Urban, M. Buballa, and J. Wambach, Phys. Rev. Lett. **88**, 042002 (2002).
[66] H. van Hees and R. Rapp, Procs. of the 22$^{\rm nd}$ Winter Workshop on Nuclear Dynamics 91 (2006), hep-ph/0604269.
[67] E. Braaten, R. D. Pisarski, and T.-C. Yuan, Phys. Rev. Lett. **64**, 2242 (1990).
[68] R. Rapp, Pramana **60**, 675 (2003).
[69] J. Casalderrey-Solana and E. V. Shuryak (2004), hep-ph/0408178.
[70] F. Cooper and G. Frye, Phys. Rev. D **10**, 186 (1974).
[71] M. Aguilar-Benitez et al., Z. Phys. C **50**, 405 (1991).
[72] D. d'Enterria, Eur. Phys. J. C **43**, 295 (2005).
[73] M. Glück, E. Reya, and A. Vogt, Z. Phys. C **67**, 433 (1995).
[74] C. Spieles et al., Eur. Phys. J. C **5**, 349 (1998).
[75] A. Adare et al. (PHENIX Collaboration), Phys. Rev. Lett. **98**, 172301 (2007).
[76] B. I. Abelev et al. (STAR Collaboration), Phys. Rev. Lett. **98**, 192301 (2007).
[77] H. van Hees, V. Greco, and R. Rapp, Phys. Rev. C **73**, 034913 (2006).
[78] R. Shahoyan [NA60 Collaboration], J. Phys. G **34**, S1029 (2007).
[79] I. G. Bearden et al. (NA44 Collaboration), Phys. Rev. Lett. **78**, 2080 (1997).
[80] H. Appelshäuser et al. (NA49 Collaboration), Eur. Phys. J. C **2**, 661 (1998).
[81] F. Antinori et al. (WA97 Collaboration), J. Phys. G **27**, 2325 (2001); J. Phys. G **33**, 403 (2007).
[82] D. Adamova et al. (CERES Collaboration), Nucl. Phys. A **714**, 124 (2003).
[83] S. Damjanovic (2006), private communication.
[84] F. Becattini, M. Gazdzicki, A. Keranen, J. Manninen, and R. Stock, Phys. Rev. C **69**, 024905 (2004).
[85] E. Schnedermann, J. Sollfrank, and U. W. Heinz, Phys. Rev. C **48**, 2462 (1993).
[86] M. I. Gorenstein, K. A. Bugaev, and M. Gazdzicki, Phys. Rev. Lett. **88**, 132301 (2002).
[87] H. Specht (2007), arXiv:0710.5433v1 [nucl-ex].
[88] R. Arnaldi et al. (NA60 Collaboration) (2007), arXiv:0711.1816 [nucl-ex].
[89] T. Renk and J. Ruppert, arXiv:hep-ph/0612113.
[90] U. W. Heinz, R. Chatterjee, E. S. Frodermann, C. Gale, and D. K. Srivastava, Nucl. Phys. A **783**, 379 (2007).
[91] N. Xu, private communication (2007).
[92] J. I. Kapusta and E. V. Shuryak, Phys. Rev. D **49**, 4694 (1994).
[93] G. David, R. Rapp, and Z. Xu (2006), nucl-ex/0611009.

[94] R. Rapp, J. Phys. G **34**, S405 (2007).
[95] P.F. Kolb, J. Sollfrank and U.W. Heinz, Phys. Rev. C **62**, 054909 (2000).
[96] S. Afanasiev et al. (PHENIX Collaboration) (2007), arXiv:0706.3034 [nucl-ex].